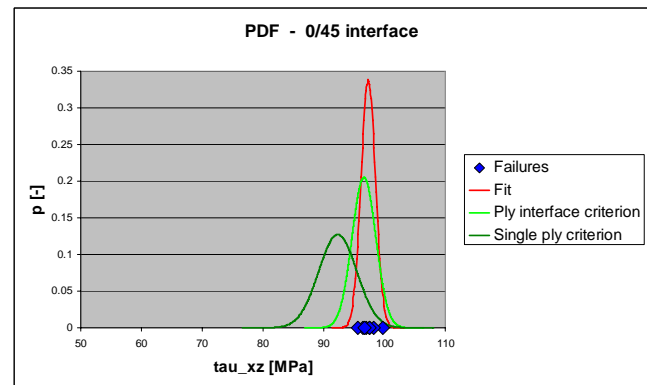
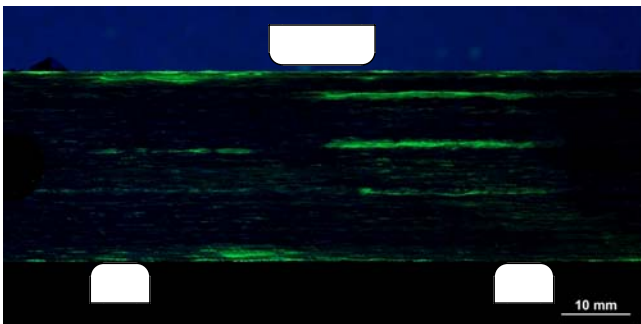




## Executive summary

# Interlaminar shear strength criteria for composites

An assessment by means of statistical analysis



### Problem area

Using the Resin Transfer Moulding (RTM) manufacturing technique, it has become possible to produce thick composite components in a cost-effective way. This enables the replacement of complex metal forgings by composite components. These components are mounted to the aircraft structure via rather thick (up to 70 mm) and heavy lugs where all loads are transferred. Besides the usual in-plane loads, large out-of-plane transverse loads may be acting on the attachment lugs as well.

The influence of transverse loads on the failure behaviour (statically and in fatigue) of thick composite structures was investigated in a 2007 Strategic Research Programme “Transverse load introduction in thick composite aircraft structures”. The programme

showed that composites are indeed sensitive to fatigue for stresses in the matrix-dominated transverse shear mode. Further, the research gave strong indications that in some cases traditional Interlaminar Shear (ILS) failure criteria are somewhat conservative.

Therefore, a supplemental in-house NLR research programme “Bezwijkcriteria voor composieten” was started in which these failure criteria are investigated into greater detail. The results are described in the current report.

### Description of work

The work can be divided in two major parts, the formulation of a new failure criterion and the evaluation of that criterion using statistical analysis.

The new criterion should result in a better representation of the failure

### Report no.

NLR-TP-2009-262

### Author(s)

R.J.C. Creemers

### Report classification

UNCLASSIFIED

### Date

February 2010

### Knowledge area(s)

Lucht- en Ruimtevaart  
Constructie- en  
Fabricagetechnologie

### Descriptor(s)

Interlaminar shear  
failure criterion  
statistical analysis  
criterion evaluation

This report is based on a presentation held at the Sicomp conference, Piteå, 8-9 June 2009.

behaviour than the traditional criteria. The supporting evidence is gathered in a test programme on ILS coupons with several different ply interfaces.

Next, a statistical analysis procedure is developed. It is used to compare the strength prediction of the new and traditional criteria with the data found by test. By doing so, any observed differences between predictions become quantifiable instead of a just a general feeling based on observation.

### **Results and conclusions**

The test results on thin ILS coupons show distinct differences for the strength of different interfaces. This was confirmed by statistical analysis of these test results. Not all differences in strength can be explained by traditional ILS criteria, such as Hashin and Kim&Soni. However, the newly formulated “ply interface” criterion is able to predict/explain these differences. The ILS strength of any arbitrary interface is calculated based on:

- The local ply stresses in both plies adjacent to the interface
- The difference in ply angles between the two plies
- The two shear strength values  $S_{13}$  and  $S_{23}$  of the 0/0 and 90/90 interface.

At first sight, application of the new criterion results in a slightly better strength prediction for certain configurations.

In order to confirm that feeling, a statistical method has been developed to evaluate different failure criteria. It is suitable for general application, so any criterion can be checked with this particular procedure. The basic assumption of this method is that in order to correctly describe the failure behaviour both variance and mean value should be predicted accurately by the criterion. This implies that there is a relation between the distributions or data scatter for different configurations, which actually exist in reality and is captured correctly by the criterion. Application of this procedure to the newly developed ply interface criterion and traditional criteria shows that the new criterion indeed performs better. This is especially the case for the 0/90 and 0/45 interfaces, or more generally for configurations with highly dissimilar ply stresses in the two plies adjacent to the interface.

### **Applicability**

The newly developed criterion is a static ILS failure criterion suitable for use in the design of any composite component in which transverse shear stresses occur. The statistical procedure for evaluation of failure criteria is even more general. Any criterion can be checked with this particular procedure. It provides evidence whether the criterion is a good representation of the actual failure behaviour.



NLR-TP-2009-262

## Interlaminar shear strength criteria for composites



### An assessment by means of statistical analysis

R.J.C. Creemers

This report is based on a presentation held at the Sicomp conference, Piteå, 8-9 June 2009.  
The contents of this report may be cited on condition that full credit is given to NLR and the author.  
This publication has been refereed by the Advisory Committee AEROSPACE VEHICLES.

Customer                      National Aerospace Laboratory NLR  
Contract number            ----  
Owner                         National Aerospace Laboratory NLR  
Division NLR                Aerospace Vehicles  
Distribution                 Unlimited  
Classification of title      Unclassified  
February 2010

Approved by:

Author	Reviewer	Managing department
 8-2-2010		13 <sup>22</sup> / <sub>1</sub> , 10



## Summary

The current report describes the results from an in-house NLR research programme “Bezwijkcriteria voor composieten” in which failure criteria are investigated to predict the Interlaminar Shear Strength of composite laminates. The work can be divided in two major parts, the formulation of a new failure criterion and the evaluation of that criterion using statistical analysis.

Test results on thin ILS coupons show distinct differences for the strength of different interfaces. Not all differences in strength can be explained by traditional ILS criteria, such as Hashin and Kim&Soni. However, the newly formulated “ply interface” criterion is able to predict/explain these differences. Also, application of the new criterion seems to result in a slightly better strength prediction for certain configurations.

In order to confirm that feeling, a statistical method has been developed to evaluate different failure criteria. It is suitable for general application, so any criterion can be checked with this particular procedure. The basic assumption of this method is that, in order to correctly describe the failure behaviour, both variance and mean value should be predicted accurately by the criterion. Application of this procedure to the newly developed ply interface criterion and traditional criteria shows that the new criterion indeed performs better. This is especially the case for the 0/90 and 0/45 interfaces, or more generally for configurations with highly dissimilar ply stresses in the two plies adjacent to the interface.

## Contents

<b>Abbreviations</b>	<b>5</b>
<b>Symbols</b>	<b>6</b>
<b>1 Introduction</b>	<b>7</b>
<b>2 Formulation of a new failure criterion</b>	<b>10</b>
2.1 Analytical derivation of transverse shear stresses	10
2.2 Interlaminar shear strength of thin test coupons	12
2.3 Interlaminar shear strength criteria	16
2.3.1 Traditional ILSS criteria	16
2.3.2 Formulation of a new ILSS criterion	18
<b>3 Evaluation of failure criteria using statistical analysis</b>	<b>23</b>
3.1 General background of statistical analysis	23
3.2 Evaluation of test results	26
3.3 Evaluation of failure criteria	29
3.3.1 Statistical procedure	29
3.3.2 Evaluation of ILS failure criteria	32
<b>4 Conclusions and recommendations</b>	<b>36</b>
<b>References</b>	<b>38</b>
<b>Appendix A The analytical determination of transverse shear stresses</b>	<b>39</b>
<b>Appendix B</b>	<b>53</b>
<b>Appendix C ILS failure stress in local ply directions</b>	<b>55</b>

## Abbreviations

ANOVA	Analysis of variance
ASTM	American Society for Testing and Materials
CFRP	Carbon Fibre Reinforced Plastic
CDF	Cumulative Density Function
CPT	Classical Plate Theory
FEM	Finite Element Method
ILS	Interlaminar Shear
ILSS	Interlaminar Shear Strength
NIVR	Nederlands Instituut voor Vliegtuigontwikkeling en Ruimtevaart
NLR	National Aerospace Laboratory NLR
PDF	Probability Density Function
RTM	Resin Transfer Moulding
SPA	Stork SP Aerospace B.V.
SRP	Strategic Research Programme
UD	Uni-Directional

## Symbols

$b$	width
$E$	modulus of elasticity
$h$	height
$L$	length
$l_v$	span length
$M$	bending moment per unit length
$N$	axial force per unit length
$P$	force, concentrated load, probability
$p$	pressure (force per unit area)
$Q$	transverse force per unit length
$S_{13}, S_{23}$	transverse shear strength in the local 13 and 23 directions of a ply, transverse shear strength of the 0/0 and 90/90 interface
$t$	thickness
$V$	shear force
$W$	width
$x, y, z$	rectangular coordinates, distances
$\varepsilon$	normal strain
$\varepsilon_1, \varepsilon_2$	normal strains in the local 11 and 22 directions of a ply
$\varepsilon_x, \varepsilon_y$	normal strains in the global x and y directions of a laminate
$\gamma$	shear strain
$\gamma_{12}, \gamma_{13}, \gamma_{23}$	shear strains in the local 12, 13 and 23 directions of a ply
$\gamma_{xy}, \gamma_{xz}, \gamma_{yz}$	shear strains in the global xy, xz and yz directions of a laminate
$\kappa$	curvature
$\nu$	Poisson's ratio
$\sigma$	normal stress
$\sigma_1, \sigma_2, \sigma_3$	normal stresses in the local 11, 22 and 33 directions of a ply
$\sigma_x, \sigma_y, \sigma_z$	normal stresses in the global x, y and z directions of a laminate
$\tau$	shear stress
$\tau_{12}, \tau_{13}, \tau_{23}$	shear stresses in the local 12, 13 and 23 directions of a ply
$\tau_{xy}, \tau_{xz}, \tau_{yz}$	shear stresses in the global xy, xz and yz directions of a laminate
$\theta$	ply angle



## 1 Introduction

Using the Resin Transfer Moulding (RTM) manufacturing technique, it has become possible to produce thick composite components in a cost-effective way. This enables the replacement of complex metal forgings by composite components, which was demonstrated in several recent technology programmes (ALCAS, NIVR CVO-ACCOLADE, CODEMA LA gear). The components investigated under these programmes are mounted to the aircraft structure via relatively thick (up to 70 mm) and heavy lugs where all loads are transferred. Besides the usual in-plane loads, large out-of-plane transverse loads may be acting on the attachment lugs as well. This is especially the case for the ALCAS Main Landing Gear support beam, but is also very relevant for torque links, trailing arms, motor pylons and any heavily loaded fitting in general, see figure 1 and figure 2.

As Carbon Fibre Reinforced Plastic (CFRP) materials show excellent strength and stiffness properties when loaded in the fibre direction, structures under in-plane loading usually outperform their metallic counterparts, especially when subjected to fatigue. However, the composite's ability to withstand out-of-plane loading is predominantly governed by the properties of the matrix, which has a much lower static strength and is much more sensitive to fatigue. This is of importance particularly for thick components. Thin components, even when loaded by a relatively small transverse load, will deform largely by bending. This causes high in-plane compressive and tensile stresses in the outer fibres of the laminate. Consequently, the strength of such components is determined by the in-plane tension and/or compression allowable of the single CFRP ply, and the transverse shear stresses may be ignored. However,

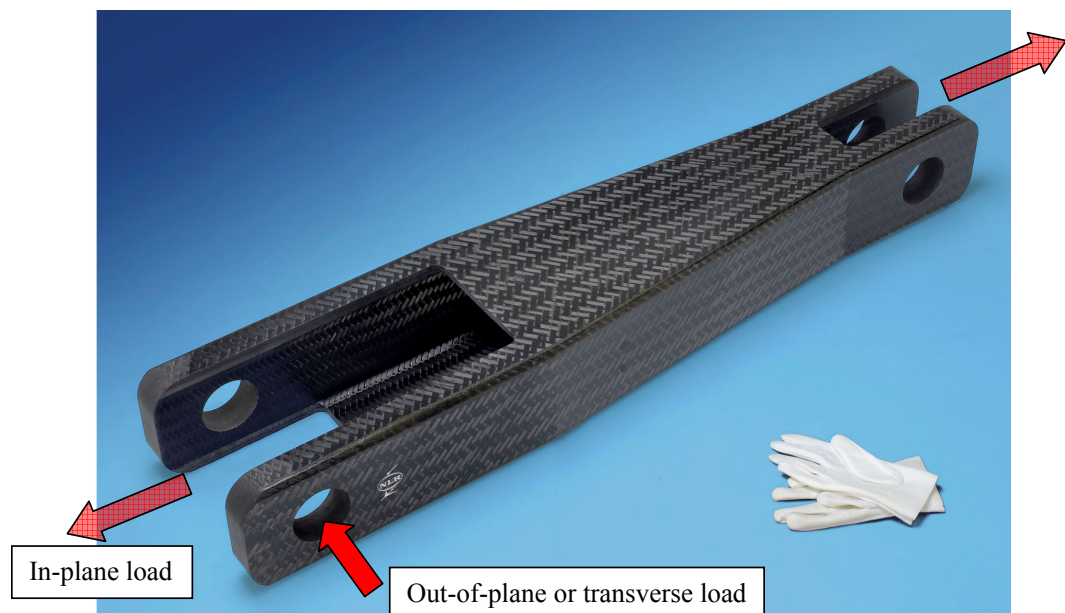
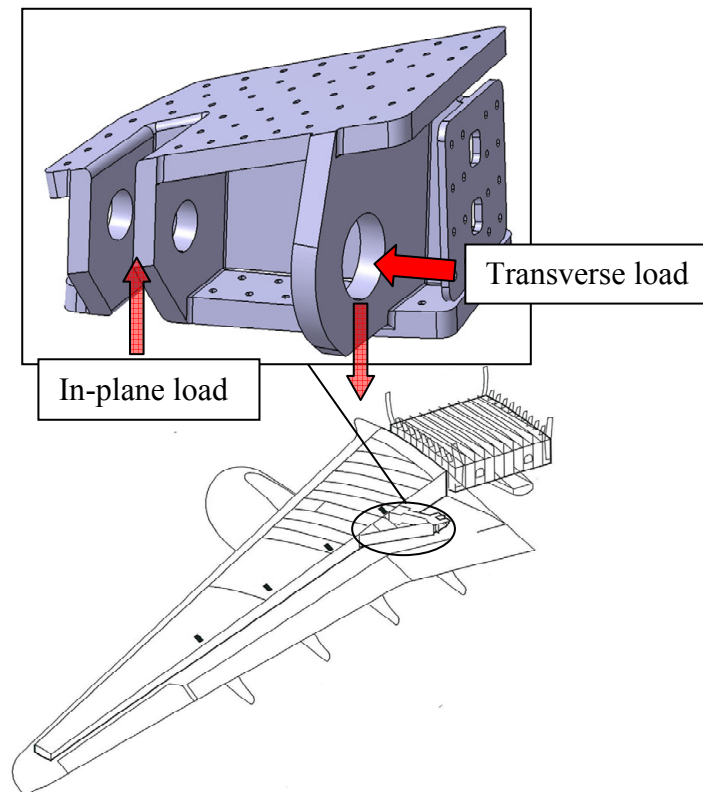


Fig. 1 ACCOLADE Generic Composite Brace and its primary load components



*Fig. 2 ALCAS Main Landing Gear support beam and its primary load components*

while the bending strength increases quadratically with the thickness, the strength in transverse direction increases only linearly. Then, the failure behaviour of thick composite structures will change under influence of the transverse shear stresses that are caused by the transverse loading. Therefore, in 2007 a Strategic Research Programme was started towards thick composites under transverse loading (Ref. 1). This programme was funded by the Netherlands Agency for Aerospace Programmes (NIVR) and Stork SP Aerospace B.V. (SPA). Also, parts of the work were performed by or in cooperation with Stork SP Aerospace B.V. The programme showed that composites are indeed sensitive to fatigue for stresses in the matrix-dominated transverse shear mode. Further, the research gave strong indications (but no hard evidence) that, although the failure location was predicted correctly, in some cases traditional Interlaminar Shear (ILS) failure criteria are too conservative, see figure 3 where the criticality analysis shows criterion values close to 1.2 for the Lecuyer criterion. This means that the strength is underestimated by almost 20 %.

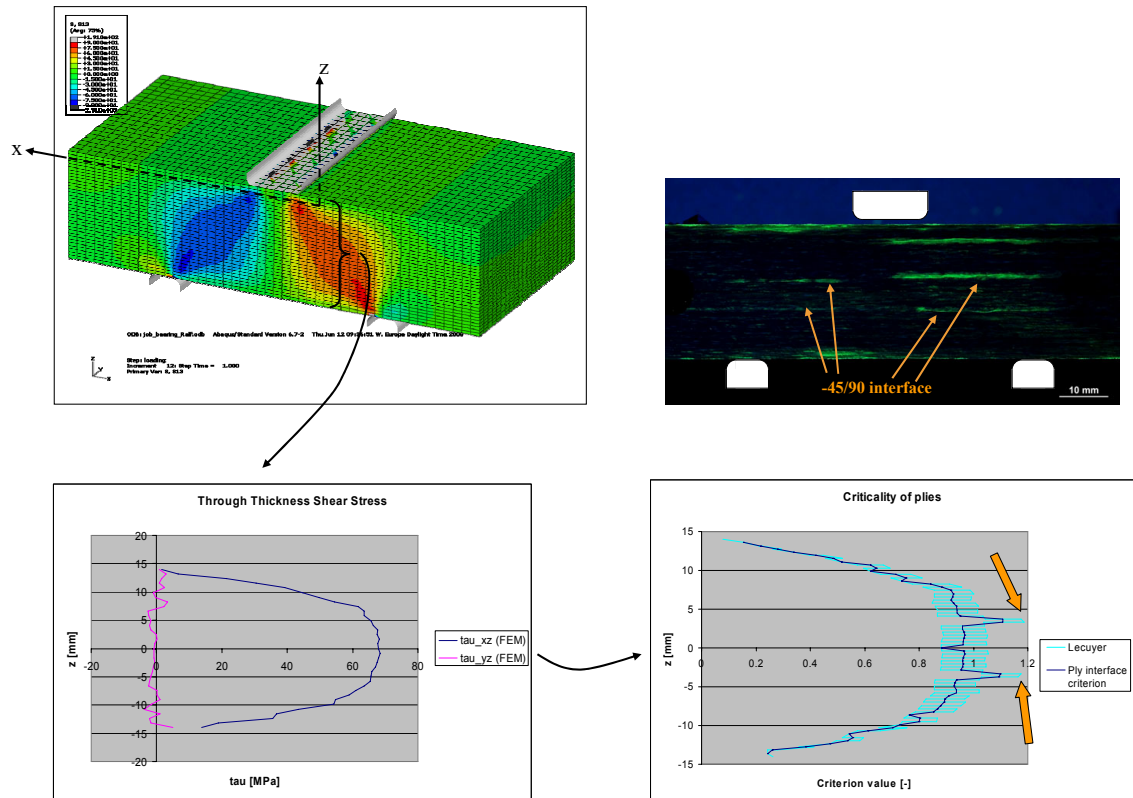


Fig. 3 Transverse shear stresses in thick coupons and criticality of the different interfaces

In order to provide the evidence that traditional failure criteria are conservative and that an alternative criterion actually performs better, a supplemental in-house NLR research programme “Bezwijkcriteria voor composieten” was started in which these failure criteria are investigated into greater detail. That work is presented in the current report. First, some additional testing is performed on uni-directional prepreg material to be used for the formulation of the new criterion in chapter 2. Next, a statistical procedure is set up to evaluate the different criteria in chapter 3. The procedure is a generic method that could be applied to any other criterion as well. Finally, in chapter 4 conclusions are drawn and recommendations are given.

## 2 Formulation of a new failure criterion

This chapter starts with an analytical derivation of the transverse shear stresses in a composite plate under transverse loading. The formulas are used to determine the failure stress in the ILS coupon tests. These test results formed the cause for the formulation of a new failure criterion.

### 2.1 Analytical derivation of transverse shear stresses

The full analytical derivation of the in-plane and transverse stresses in a flat plate is presented in Appendix A, see reference 1 as well. The most important results are summarised in this paragraph for both an isotropic and a composite flat plate/beam.

All formulas have been derived under the condition that only forces in the x-direction are considered without gradients in y-direction. Any loads in transverse direction are applied to the top surface and normal to that surface.

#### Strains and stresses in an isotropic plate/beam

For an isotropic flat plate or beam with only loads applied in x-direction or to the top surface and normal to that surface, the formulas for the in-plane strains and stresses become:

$$\begin{aligned}
 \varepsilon_x &= \frac{N_x}{E \cdot h} + 12 \cdot \frac{M_x}{E \cdot h^3} \cdot z & \sigma_x &= \frac{N_x}{h} + 12 \cdot \frac{M_x}{h^3} \cdot z \\
 \varepsilon_y &= -\nu \cdot \varepsilon_x & \sigma_y &= 0 \\
 \gamma_{xy} &= 0 & \tau_{xy} &= 0
 \end{aligned}
 \tag{Eq. 1}$$

The through-thickness stresses can be calculated with:

$$\begin{aligned}
 \sigma_z &= \frac{1}{2} \cdot p \cdot \left( 1 + 3 \cdot \frac{z}{h} - 4 \cdot \left( \frac{z}{h} \right)^3 \right) \\
 \tau_{xz} &= \frac{3}{2} \frac{Q_x}{h} \cdot \left( 1 - \left( \frac{2 \cdot z}{h} \right)^2 \right) \\
 \tau_{yz} &= 0
 \end{aligned}
 \tag{Eq. 2}$$

Eq. 1 clearly shows that for isotropic materials the stress components  $\sigma_y$  and  $\tau_{xy}$  are zero through the entire thickness, while  $\sigma_x$  varies linearly with the z-coordinate. Notice that strains (and curvature) in y-direction are not zero due to the Poisson's effect.

The through-thickness normal stress  $\sigma_z$  is defined by a third order polynomial. The maximum through-thickness normal stress is found at the upper surface (where the load is applied) and is equal to  $\sigma_z = p$  which is exactly the applied surface load. The through-thickness shear stress

$\tau_{xz}$  has a parabolic distribution through the thickness. The maximum is found in the middle of the plate/beam at  $z = 0$  and is equal to  $\tau_{xz} = \frac{3}{2} Q_x / h$ .

### Strains and stresses in a composite plate/beam

The well-known formula according to Classical Laminate Theory is presented by:

$$\begin{Bmatrix} N_x \\ N_y \\ N_{xy} \\ M_x \\ M_y \\ M_{xy} \end{Bmatrix} = \begin{bmatrix} A_{11} & A_{12} & A_{16} & B_{11} & B_{12} & B_{16} \\ A_{21} & A_{22} & A_{26} & B_{21} & B_{22} & B_{26} \\ A_{61} & A_{62} & A_{66} & B_{61} & B_{62} & B_{66} \\ B_{11} & B_{12} & B_{16} & D_{11} & D_{12} & D_{16} \\ B_{21} & B_{22} & B_{26} & D_{21} & D_{22} & D_{26} \\ B_{61} & B_{62} & B_{66} & D_{61} & D_{62} & D_{66} \end{bmatrix} \cdot \begin{Bmatrix} \bar{\varepsilon}_x \\ \bar{\varepsilon}_y \\ \bar{\gamma}_{xy} \\ \bar{\kappa}_x \\ \bar{\kappa}_y \\ 2 \cdot \bar{\kappa}_{xy} \end{Bmatrix} \quad \text{Eq. 3}$$

With:

$$\begin{aligned} A_{ij} &= \sum_{k=1}^n (\bar{C}_{ij})_{(k)} \cdot (z_k - z_{k-1}) \\ B_{ij} &= \frac{1}{2} \cdot \sum_{k=1}^n (\bar{C}_{ij})_{(k)} \cdot (z_k^2 - z_{k-1}^2) \\ D_{ij} &= \frac{1}{3} \cdot \sum_{k=1}^n (\bar{C}_{ij})_{(k)} \cdot (z_k^3 - z_{k-1}^3) \end{aligned}$$

After inversion of the  $ABD$ -matrix, here denoted as  $abd$  with components  $a_{ij}$ ,  $b_{ij}$ , and  $d_{ij}$ , the strains and stresses can be calculated in both the global coordinate system and in the local ply coordinate system (under the condition that all applied loads in y-direction are zero):

$$\begin{aligned} \begin{Bmatrix} \varepsilon_x \\ \varepsilon_y \\ \gamma_{xy} \end{Bmatrix} &= \begin{Bmatrix} a_{11} + b_{11} \cdot z \\ a_{21} + b_{21} \cdot z \\ a_{61} + b_{61} \cdot z \end{Bmatrix} \cdot N_x + \begin{Bmatrix} b_{11} + d_{11} \cdot z \\ b_{21} + d_{21} \cdot z \\ b_{61} + d_{61} \cdot z \end{Bmatrix} \cdot M_x \\ \begin{Bmatrix} \varepsilon_1 \\ \varepsilon_2 \\ \gamma_{12} \end{Bmatrix}_{(k)} &= [T]_{(k)}^{-T} \cdot \begin{Bmatrix} \varepsilon_x \\ \varepsilon_y \\ \gamma_{xy} \end{Bmatrix} \\ \begin{Bmatrix} \sigma_x \\ \sigma_y \\ \tau_{xy} \end{Bmatrix}_{(k)} &= [\bar{C}]_{(k)} \cdot \begin{Bmatrix} \varepsilon_x \\ \varepsilon_y \\ \gamma_{xy} \end{Bmatrix} \\ \begin{Bmatrix} \sigma_1 \\ \sigma_2 \\ \tau_{12} \end{Bmatrix}_{(k)} &= [C]_{(k)} \cdot \begin{Bmatrix} \varepsilon_1 \\ \varepsilon_2 \\ \gamma_{12} \end{Bmatrix}_{(k)} \end{aligned} \quad \text{Eq. 4}$$

The through-thickness stresses can be calculated with:

$$\begin{aligned}
 \tau_{xz}^{(k)} &= - \sum_{j=1}^{k-1} \left\{ \left( \bar{C}_{11(j)} \cdot b_{11} + \bar{C}_{12(j)} \cdot b_{21} + \bar{C}_{16(j)} \cdot b_{61} \right) \cdot (z_j - z_{j-1}) \right. \\
 &\quad \left. + \frac{1}{2} \cdot \left( \bar{C}_{11(j)} \cdot d_{11} + \bar{C}_{12(j)} \cdot d_{21} + \bar{C}_{16(j)} \cdot d_{61} \right) \cdot (z_j^2 - z_{j-1}^2) \right\} \cdot Q_x \\
 &\quad - \left\{ \left( \bar{C}_{11(k)} \cdot b_{11} + \bar{C}_{12(k)} \cdot b_{21} + \bar{C}_{16(k)} \cdot b_{61} \right) \cdot (z - z_{k-1}) \right. \\
 &\quad \left. + \frac{1}{2} \cdot \left( \bar{C}_{11(k)} \cdot d_{11} + \bar{C}_{12(k)} \cdot d_{21} + \bar{C}_{16(k)} \cdot d_{61} \right) \cdot (z^2 - z_{k-1}^2) \right\} \cdot Q_x \\
 \\
 \tau_{yz}^{(k)} &= - \sum_{j=1}^{k-1} \left\{ \left( \bar{C}_{61(j)} \cdot b_{11} + \bar{C}_{62(j)} \cdot b_{21} + \bar{C}_{66(j)} \cdot b_{61} \right) \cdot (z_j - z_{j-1}) \right. \\
 &\quad \left. + \frac{1}{2} \cdot \left( \bar{C}_{61(j)} \cdot d_{11} + \bar{C}_{62(j)} \cdot d_{21} + \bar{C}_{66(j)} \cdot d_{61} \right) \cdot (z_j^2 - z_{j-1}^2) \right\} \cdot Q_x \\
 &\quad - \left\{ \left( \bar{C}_{61(k)} \cdot b_{11} + \bar{C}_{62(k)} \cdot b_{21} + \bar{C}_{66(k)} \cdot b_{61} \right) \cdot (z - z_{k-1}) \right. \\
 &\quad \left. + \frac{1}{2} \cdot \left( \bar{C}_{61(k)} \cdot d_{11} + \bar{C}_{62(k)} \cdot d_{21} + \bar{C}_{66(k)} \cdot d_{61} \right) \cdot (z^2 - z_{k-1}^2) \right\} \cdot Q_x \\
 \\
 \sigma_z^{(k)} &= \sigma_z^{(k-1)}(z = z_{k-1}) - \sum_{j=1}^{k-1} \left\{ \left( \bar{C}_{11(j)} \cdot b_{11} + \bar{C}_{12(j)} \cdot b_{21} + \bar{C}_{16(j)} \cdot b_{61} \right) \cdot (z_j - z_{j-1}) \right. \\
 &\quad \left. + \frac{1}{2} \cdot \left( \bar{C}_{11(j)} \cdot d_{11} + \bar{C}_{12(j)} \cdot d_{21} + \bar{C}_{16(j)} \cdot d_{61} \right) \cdot (z_j^2 - z_{j-1}^2) \right\} \cdot (z - z_{k-1}) \cdot p \\
 &\quad - \left\{ \frac{1}{2} \cdot \left( \bar{C}_{11(k)} \cdot b_{11} + \bar{C}_{12(k)} \cdot b_{21} + \bar{C}_{16(k)} \cdot b_{61} \right) \cdot (z - z_{k-1})^2 \right. \\
 &\quad \left. + \frac{1}{6} \cdot \left( \bar{C}_{11(k)} \cdot d_{11} + \bar{C}_{12(k)} \cdot d_{21} + \bar{C}_{16(k)} \cdot d_{61} \right) \cdot (z - z_{k-1})^2 \cdot (z + 2 \cdot z_{k-1}) \right\} \cdot p
 \end{aligned}
 \tag{Eq. 5}$$

Eq. 4 and Eq. 5 completely define the stress state in a beam (under the condition that any surface load is applied to the top surface and normal to that surface). The through-thickness shear stress  $\tau_{xz}$  has a parabolic distribution through the thickness of each layer. The (global) distribution through the laminate depends on the lay-up. This is shown in Appendix B.

## 2.2 Interlaminar shear strength of thin test coupons

All tests are done on laminates made from uni-directional (UD) prepreg material Hexply NCHR 913/35 %/132/HTA7 with nominal ply thickness 0.124 mm ( $V_f = 60\%$ ). To determine the influence of fibre orientations and the different ply interfaces on the interlaminar shear strength, interlaminar shear test are done on specimens with different lay-ups as given in table 1. Not all specimens were tested, only eight per configuration.

*Table 1 Different lay-ups for shear strength determination*

Specimen	Number	Notation	Lay-up	Failure location
Config 1	1/12	0/0	0 <sub>16</sub> ,0,0,0,0,0,0 <sub>16</sub>	0/0 interface
Config 2	13/24	0/90	0 <sub>16</sub> ,0,0,90,0,0,0 <sub>16</sub>	0/90 interface
Config 3	25/36	0/45	0 <sub>16</sub> ,0,0,45,0,0,0 <sub>16</sub>	0/45 interface
Config 4	37/48	45/90	0 <sub>16</sub> ,0,45,90,45,0,0 <sub>16</sub>	45/90 interface
Config 5	49/60	45/45	0 <sub>16</sub> ,0,45,45,45,0,0 <sub>16</sub>	45/45 interface
Config 6	61/72	-45/45	0 <sub>16</sub> ,0,45,-45,45,0,0 <sub>16</sub>	-45/45 interface
Config 7	73/84	90/90 <sup>1</sup>	0 <sub>16</sub> ,0,90,90,90,0,0 <sub>16</sub>	90/90 interface
Config 8	85/96	90/90 <sup>2</sup>	0 <sub>16</sub> ,45,90,90,90,45,0 <sub>16</sub>	90/90 interface
Config 9	97/108	-30/30	0 <sub>16</sub> ,0,30,-30,30,0,0 <sub>16</sub>	-30/30 interface
Config 10	109/120	-60/60	0 <sub>16</sub> ,0,60,-60,60,0,0 <sub>16</sub>	-60/60 interface
Config 11	121/132	30/30	0 <sub>16</sub> ,0,30,30,30,0,0 <sub>16</sub>	30/30 interface
Config 12	133/144	60/60	0 <sub>16</sub> ,0,60,60,60,0,0 <sub>16</sub>	60/60 interface

Figure 4 gives the specimen configuration and the test set-up. The tests at RT are carried out under laboratory conditions at ambient temperature, typically 22 °C. Before testing, the actual thickness and the width of the specimens are measured in the middle of the specimen. All specimens are tested in the 250 kN Scheck Trebel test machine with a 50 kN load cell under displacement rate control. The crosshead displacement rate of the test machine was 1.0 mm/min. The span ( $l_v$ ) between the centres of the supports of the test fixture was 18 mm (approximately 4 times the thickness). The displacement and load signals are logged during the tests.

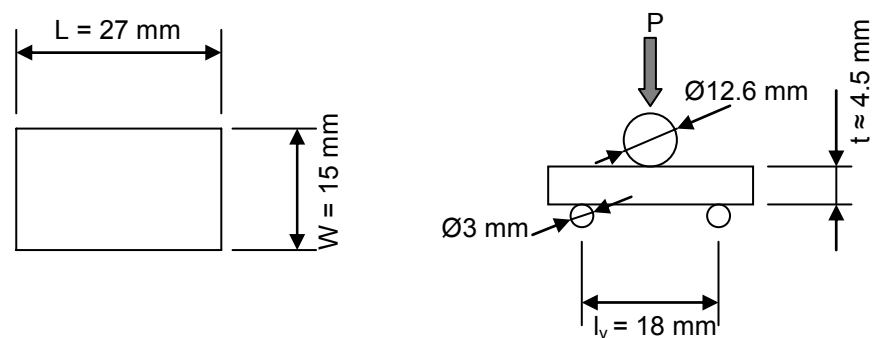


*Fig. 4 Specimen configuration and schematic test set-up*

All specimens failed in a catastrophic mode. After the first load drop, the specimens did no longer have any load carrying capabilities. The maximum load is used to determine the shear stress at the critical interface. This requires the use of the measured thickness and width of the specimens in combination with the formula for transverse shear stresses (Eq. 5) as derived in the previous paragraph, because the stress distribution depends on the lay-up. This is shown in figure 5(a) where the “soft” inner plies of configuration 8 result in a slightly blunter curve for the transverse shear stresses. The stresses in global laminate direction can of course be transferred to local ply stresses, see figure 5(b). It shows that the three inner 90° plies are mainly loaded in shear in their local 23-direction, while shear stresses in 13-direction are (very close to) zero.

The failure stress  $\tau_{xz}$  in the critical interface is given for all specimens in figure 6. The blue diamonds are the individual test results. The red cross is the mean value of each configuration and the red bars give the upper and lower bounds for 90 % coverage with 95 % confidence interval (B-basis confidence level). It can be seen that both the mean value and scatter differ between configurations. As one would expect, the 0/0 interface shows the highest strength, while the 90/90 interface shows the lowest strength.

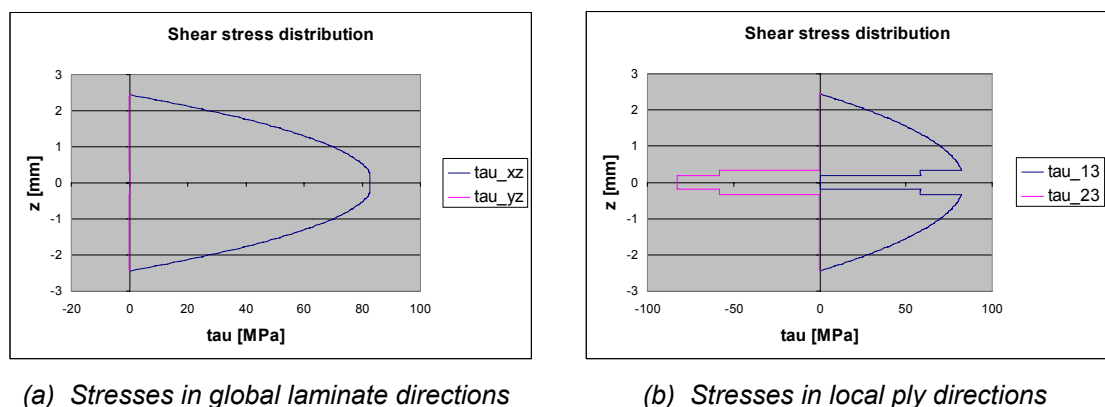


Fig. 5 Shear stress distribution in specimen V8-1 with lay-up  $[0_{16}, 45, 90, 90, 90, 45, 0_{16}]$



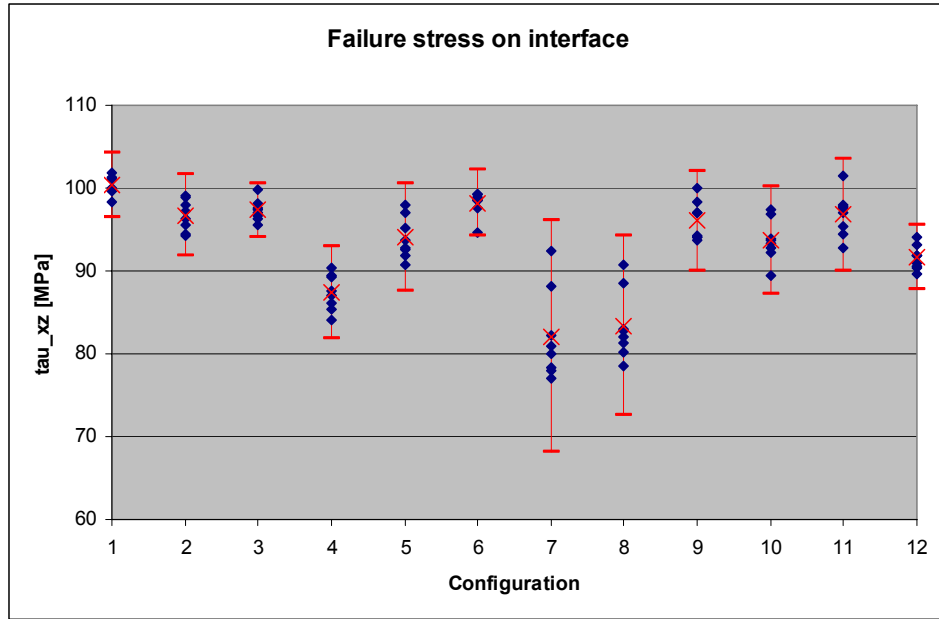


Fig. 6 Failure stress on the critical interface for all ILS specimens

As mentioned above, the shear stresses in global laminate direction can be transferred to their local ply directions. The following equations have to be applied for the two plies adjacent to the critical interface:

$$\begin{aligned}
 \tau_{13,\text{ply}1} &= \tau_{xz,\text{ply}1} \cdot \cos \theta_1 + \tau_{yz,\text{ply}1} \cdot \sin \theta_1 \\
 \tau_{23,\text{ply}1} &= -\tau_{xz,\text{ply}1} \cdot \sin \theta_1 + \tau_{yz,\text{ply}1} \cdot \cos \theta_1 \\
 \tau_{13,\text{ply}2} &= \tau_{xz,\text{ply}2} \cdot \cos \theta_2 + \tau_{yz,\text{ply}2} \cdot \sin \theta_2 \\
 \tau_{23,\text{ply}2} &= -\tau_{xz,\text{ply}2} \cdot \sin \theta_2 + \tau_{yz,\text{ply}2} \cdot \cos \theta_2
 \end{aligned}$$

Eq. 6

When both plies adjacent to the interface have identical ply angles ( $\theta/\theta$  interface), the stresses in both plies are the same. The local ply stresses in those configurations are shown in figure 7. For interfaces of plies with dissimilar ply angles, different local ply stresses occur in the two plies, so these have to be plotted separately. Appendix B shows these local ply stresses in both plies. Different configurations have been combined in a single picture. According to figure C-1 and figure C-2 there appears to be an elliptical correlation between  $\tau_{13}$  and  $\tau_{23}$  for both the  $\theta/\theta$  interface and the  $\theta/\theta$  interface. Further, close investigation of figure C-3, figure C-4 and figure C-5, shows that failure of the  $0/\theta$ ,  $45/\theta$  and  $90/\theta$  interface seems not to depend solely on the stresses in respectively the  $0^\circ$ ,  $45^\circ$  and  $90^\circ$  ply. For instance, when looking at the failure stress in the  $45^\circ$  ply in figure C-4, it is possible to distinguish the three different groups with the  $0/45$ ,  $45/45$  and  $45/90$  interfaces. This indicates that failure does not depend on the stress in the  $45^\circ$  ply alone; the strength of the interface is influenced by the other ply as well.

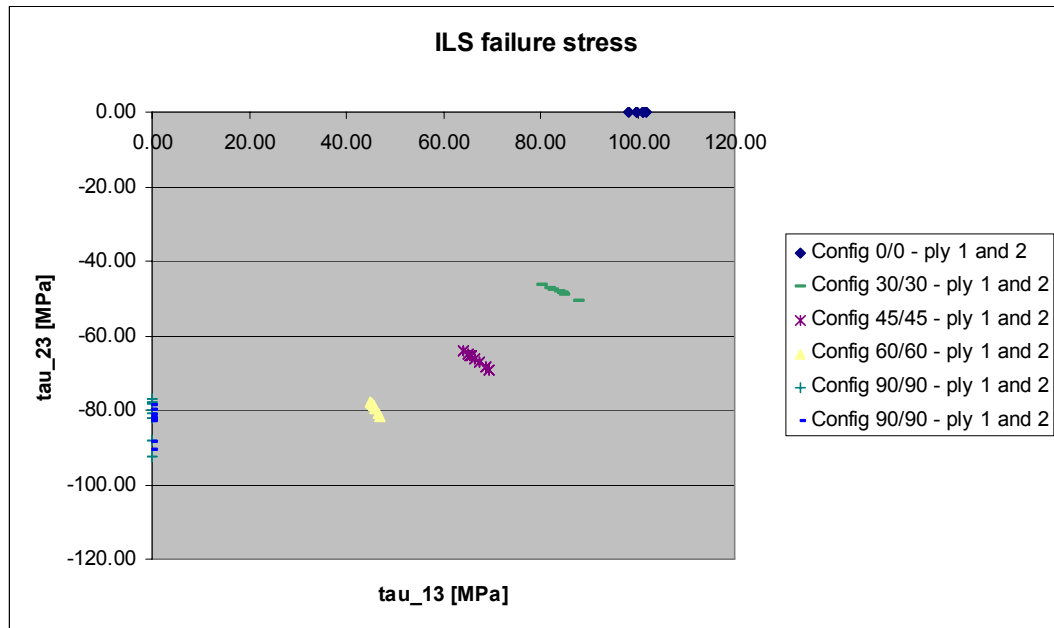


Fig. 7 Failure stress in local ply directions for  $\theta/\theta$  interface

### 2.3 Interlaminar shear strength criteria

In this section, an overview is given of traditional failure criteria and why they fail to predict the strength of all interfaces correctly. This has resulted in the formulation of a new failure criterion for the interlaminar shear strength.

#### 2.3.1 Traditional ILSS criteria

Reference 1 gives a more extensive overview of failure criteria, such as Puck, Chamis, Tsai-Wu, Christensen, Hashin, Kim and Soni, Brewer and Lagace, and Lecuyer. Investigation of these criteria shows that both Tsai-Wu and Christensen include transverse shear stresses in their criteria. However, the transverse shear strength is assumed to be enclosed in the axial shear strength ( $F_{66}$  in Tsai-Wu,  $\beta_1$  in Christensen) and in the transverse normal strength ( $F_{22}$  in Tsai-Wu,  $\alpha_1$  in Christensen). The transverse shear strength is not used separately in these criteria. It seems that both criteria assume that any transverse shear stress component promotes axial shear failures, but transverse shearing is not considered as a failure mode itself. Hashin, Kim and Soni, Brewer and Lagace, and Lecuyer all consider transverse stresses ( $\tau_{13}$ ,  $\tau_{23}$ ,  $\sigma_{22}$ ,  $\sigma_{33}$ ) and transverse strengths ( $S_{13}$ ,  $S_{23}$ ,  $S_{22}$ ,  $S_{33}$ ) in their criteria. When only transverse shear stresses are considered and other stress components are neglected, all criteria reduce to the following form:

$$\frac{\tau_{13}^2}{S_{13}^2} + \frac{\tau_{23}^2}{S_{23}^2} \leq 1 \quad \text{Eq. 7}$$

Generally, the  $S_{23}$  strength of a uni-directional ply is smaller than the  $S_{13}$  strength.

Although the criteria all look the same their application is quite different, because the Hashin criterion is associated with lamina failures, while Kim and Soni, Brewer and Lagace, and Lecuyer are associated with out-of-lamina failures. The first approach (lamina failures) considers the shear stress components within each single ply in the laminate separately. The strength of the laminate is determined by the most critically loaded ply. So this results in a search for the weakest ply. However, the criterion cannot reproduce some of the dissimilar ply interface strengths observed in the coupon tests of figure 6:

- that the 0/45-interface is stronger than the 45/45-interface under shear loading in laminate xz-direction
- that the 0/90 interface is stronger than the 45/90 interface which in turn is stronger than the 90/90 interface under shear loading in laminate xz-direction

The Hashin criterion will identify the 45° ply as the weakest ply in the first case and the 90° ply in the second case. Therefore, the predicted strength will be the same for a 0/45 as for a 45/45 laminate. Also, the predicted strength will be the same for a 0/90, a 45/90 and a 90/90 laminate. The strength depends on a single ply only and not on the stresses and orientation of both plies adjacent to the interface. This is justifiable, because Hashin assumes lamina failure. However, this makes the criterion unsuitable to predict the strength of all the interfaces, because test results seem to suggest that the interface strength depends on both plies.

As the second approach assumes out-of-lamina failures, these criteria do result in a strength prediction for the interface. The criteria are usually applied to predict the onset of edge delaminations by considering average interlaminar stresses in the interface computed on a critical length. These average stresses are applied in a failure criterion in combination with the transverse strengths. The transverse strengths are determined experimentally. They are the strengths of the interface, usually in global laminate direction (not local ply directions). They therefore depend on the laminate lay-up or ply angles at both sides of the interface, which is exactly what is observed in the ILS test results of figure 6; the interface strength depends on the orientation of both plies. In other words, the experimentally determined transverse strength values are only valid for a specific ply interface. For an accurate failure prediction, application of these out-of-lamina failure criteria is limited to a certain family of laminates, e.g.  $[\pm\theta_n]_s$  laminates with ( $5^\circ < \theta < 30^\circ$ ). For general application of these criteria in a composite structure, transverse strength values would have to be determined for all different ply interfaces of all laminates in the structure. This is of course not very practical.

So, it must be concluded that, theoretically, the failure criterion of Eq. 7 can not give an accurate prediction of the strength of all the interfaces of figure 6, either because lamina failures are assumed (not taking into account both plies adjacent to the interface), or because the tested interfaces are not all part of the same family of laminates.

When the failure criterion of Eq. 7 is applied anyway, the criterion values of figure 8 are found. They have been determined using the local ply failure stresses  $\tau_{13}$  and  $\tau_{23}$  in each specimen, calculated according to paragraph 2.1 and 2.2. The strength values for  $S_{13}$  and  $S_{23}$  are based on the two test configurations with the 0/0 and the 90/90<sup>2</sup> interface. The average strength values are used, and these are equal to respectively 100.3 MPa and 83.4 MPa.

In figure 8, a value exceeding 1.0 implies that, according to the criterion, failure should already have occurred. A value below 1.0 implies that failure was not yet expected. Naturally, for configurations 1 and 8 the average criterion value is equal to exactly 1.0, because these strength values were used as input. At first sight, the strength prediction seems quite accurate; all values are fairly close to 1.0. A more detailed investigation, however, shows that the strength of especially the 0/90 interface is somewhat underestimated. As argued above, this is exactly what one would expect with this criterion. Equal strengths are predicted for the 90/90 and 0/90 interface, whereas test results show a higher strength for the 0/90 configuration. This confirms the above-formulated suspicion that the failure criterion of Eq. 7 cannot give an accurate strength prediction for all interfaces. Therefore, in the next section a new criterion is developed.

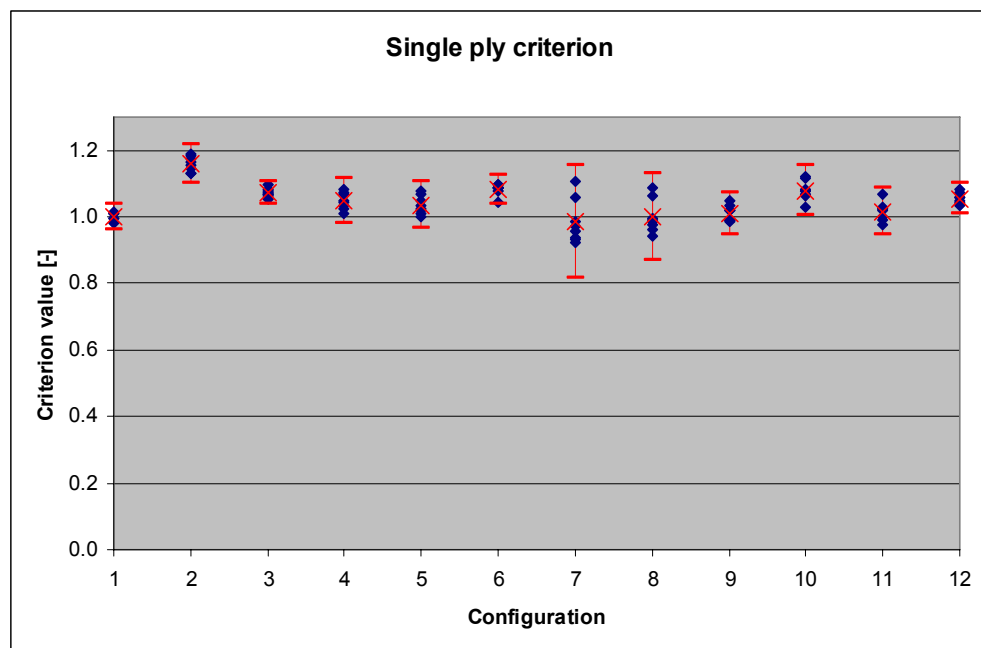
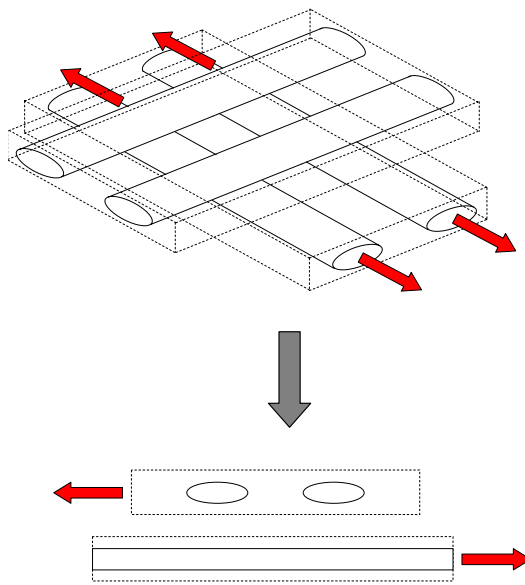
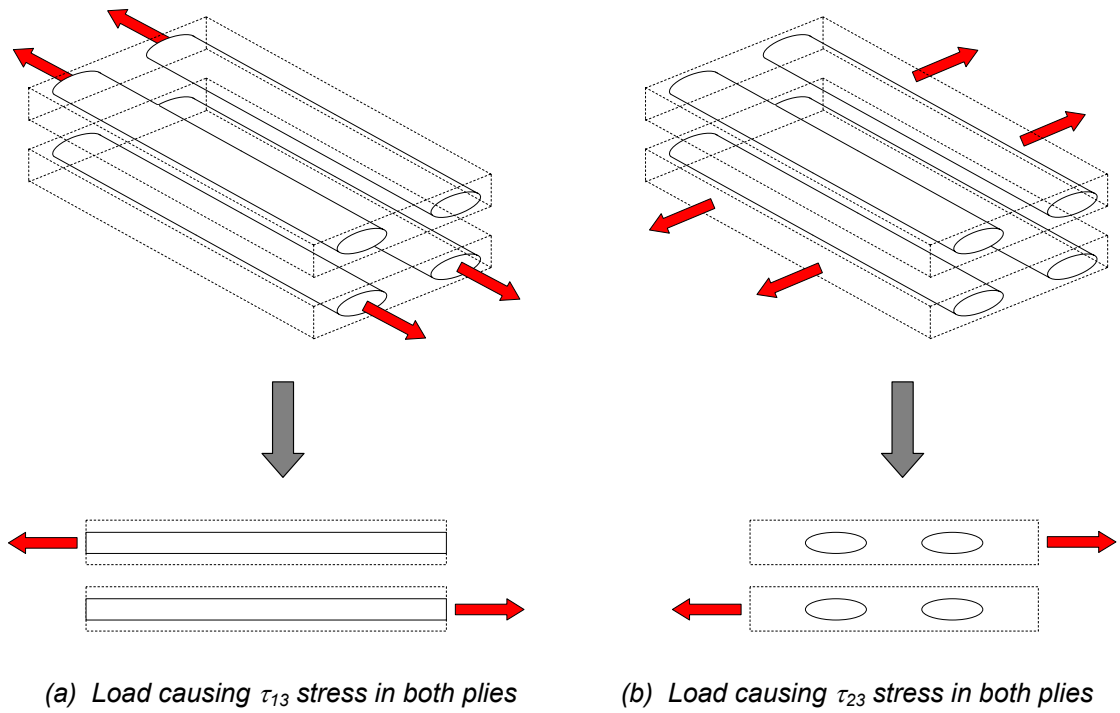


Fig. 8 Value of the failure criterion using the mean strengths of the 0/0 and 90/90<sup>2</sup> interface

### 2.3.2 Formulation of a new ILSS criterion

From the ILS test results it was observed that cracks mainly occur in the interface in between plies and not or less within the ply. It is conceived that the interface is weaker than the ply itself. Therefore, in the new failure criterion the stresses in the interface between two plies will be used to predict interlaminar shear failures.



(c) Load causing  $\tau_{13}$  stress in bottom ply and  $\tau_{23}$  stress in top ply

Fig. 9 Different loads causing different shear stresses in the plies adjacent to the interface

Figure 9 shows different types of loading on different types of laminates. These cause different ply stresses, i.e. shear stress  $\tau_{13}$  in both plies (a), shear stress  $\tau_{23}$  in both plies (b), or shear stress  $\tau_{13}$  in bottom ply and shear stress  $\tau_{23}$  in top ply (c). These ply stresses also result in stresses in the ply interface. Figure 9(a) and (b) show that there is a distinct difference between  $\tau_{13}$  and  $\tau_{23}$  loading. Therefore, it becomes self-evident to assume that the local ply stresses  $\tau_{13}$  and  $\tau_{23}$  each cause different stresses in the interface according to stress concentration factors  $K_1$  and  $K_2$ , respectively. This gives the following interface stresses in global xz- and yz-directions:

$$\begin{aligned}
 \tau_{xz,ply1} &= K_1 \cdot \tau_{13,ply1} \cdot \cos \theta_1 - K_2 \cdot \tau_{23,ply1} \cdot \sin \theta_1 \\
 \tau_{yz,ply1} &= K_1 \cdot \tau_{13,ply1} \cdot \sin \theta_1 + K_2 \cdot \tau_{23,ply1} \cdot \cos \theta_1 \\
 \tau_{xz,ply2} &= K_1 \cdot \tau_{13,ply2} \cdot \cos \theta_2 - K_2 \cdot \tau_{23,ply2} \cdot \sin \theta_2 \\
 \tau_{yz,ply2} &= K_1 \cdot \tau_{13,ply2} \cdot \sin \theta_2 + K_2 \cdot \tau_{23,ply2} \cdot \cos \theta_2
 \end{aligned}
 \tag{Eq. 8}$$

Further, it is assumed that each ply adjacent to the interface contributes to the total stress according to its own local stress state. The cumulative stress in the interface is found by combining the global stress components caused by both plies:

$$\begin{aligned}
 \tau_{xz} &= \tau_{xz,ply1} + \tau_{xz,ply2} \\
 \tau_{yz} &= \tau_{yz,ply1} + \tau_{yz,ply2}
 \end{aligned}
 \tag{Eq. 9}$$

Next, the stress components are combined in an invariant stress, similar to Von Mises. The invariant stress is calculated with:

$$\sigma^2 = 3 \cdot (\tau_{xz}^2 + \tau_{yz}^2)
 \tag{Eq. 10}$$

Substitution of Eq. 8 into Eq. 9 and into Eq. 10 results in:

$$\begin{aligned}
 \sigma^2 &= 3 \cdot K_1^2 \cdot (\tau_{13,ply1}^2 + 2 \cdot \tau_{13,ply1} \cdot \tau_{13,ply2} \cdot \cos(\theta_1 - \theta_2) + \tau_{13,ply2}^2) + \\
 &\quad 3 \cdot 2 \cdot K_1 \cdot K_2 \cdot (\tau_{13,ply1} \cdot \tau_{23,ply2} - \tau_{13,ply2} \cdot \tau_{23,ply1}) \cdot \sin(\theta_1 - \theta_2) + \\
 &\quad 3 \cdot K_2^2 \cdot (\tau_{23,ply1}^2 + 2 \cdot \tau_{23,ply1} \cdot \tau_{23,ply2} \cdot \cos(\theta_1 - \theta_2) + \tau_{23,ply2}^2)
 \end{aligned}
 \tag{Eq. 11}$$

The invariant stress is used in the following failure criterion:

$$\frac{\sigma^2}{S^2} \leq 1
 \tag{Eq. 12}$$

At least two test configurations are necessary to determine the unknown stress concentration factors  $K_1$  and  $K_2$ . Usually one selects a test configuration with only shear stresses in the 13-direction, and another configuration with only shear stresses in the 23-direction. In other words, the shear strength of a 0/0 interface and of a 90/90 interface is determined:

$$\begin{array}{l}
 \left. \begin{array}{l}
 \text{0/0 interface : ply 1 : } \tau_{13,\text{ply 1}} = S_{13} \\
 \tau_{23,\text{ply 1}} = 0 \\
 \text{ply 2 : } \tau_{13,\text{ply 2}} = S_{13} \\
 \tau_{23,\text{ply 2}} = 0 \\
 \theta_1 = \theta_2 = 0^\circ
 \end{array} \right\} \rightarrow 3 \cdot K_1^2 \cdot 4 \cdot S_{13}^2 = S^2 \rightarrow K_1^2 = \frac{1}{3} \cdot \frac{S^2}{4 \cdot S_{13}^2} \\
 \\
 \left. \begin{array}{l}
 \text{90/90 interface : ply 1 : } \tau_{13,\text{ply 1}} = 0 \\
 \tau_{23,\text{ply 1}} = S_{23} \\
 \text{ply 2 : } \tau_{13,\text{ply 2}} = 0 \\
 \tau_{23,\text{ply 2}} = S_{23} \\
 \theta_1 = \theta_2 = 90^\circ
 \end{array} \right\} \rightarrow 3 \cdot K_2^2 \cdot 4 \cdot S_{23}^2 = S^2 \rightarrow K_2^2 = \frac{1}{3} \cdot \frac{S^2}{4 \cdot S_{23}^2}
 \end{array}$$

When this is substituted into Eq. 11 and into the criterion of Eq. 12 the following criterion is found for the strength of the ply interface:

$$\begin{aligned}
 & \frac{\tau_{13,\text{ply 1}}^2 + 2 \cdot \tau_{13,\text{ply 1}} \cdot \tau_{13,\text{ply 2}} \cdot \cos(\theta_1 - \theta_2) + \tau_{13,\text{ply 2}}^2}{4 \cdot S_{13}^2} + \\
 & \frac{(\tau_{13,\text{ply 1}} \cdot \tau_{23,\text{ply 2}} - \tau_{13,\text{ply 2}} \cdot \tau_{23,\text{ply 1}}) \cdot \sin(\theta_1 - \theta_2)}{2 \cdot S_{13} \cdot S_{23}} + \\
 & \frac{\tau_{23,\text{ply 1}}^2 + 2 \cdot \tau_{23,\text{ply 1}} \cdot \tau_{23,\text{ply 2}} \cdot \cos(\theta_1 - \theta_2) + \tau_{23,\text{ply 2}}^2}{4 \cdot S_{23}^2} \leq 1
 \end{aligned} \tag{Eq. 13}$$

According to the newly defined criterion, interlaminar shear failure of the interface depends on:

- the local ply stresses  $\tau_{13}$  and  $\tau_{23}$  in both plies adjacent to the interface
- the difference in ply angles between both plies
- the two shear strength values  $S_{13}$  and  $S_{23}$  of the 0/0 and 90/90 interface

Notice that the ply interface criterion of Eq. 13 reduces to the same form as the single ply criterion of Eq. 7 for lamina failures in case both plies adjacent to the interface have the same ply angle  $\theta_1 = \theta_2$ . Also, when the out-of-lamina strength of a specific interface is used as input to deduce the two shear strength values  $S_{13}$  and  $S_{23}$  of the 0/0 and 90/90 interface, exactly the same (elliptical) strength distribution for the interface is found as predicted by the Eq. 7. But, the criterion of Eq. 7 is only valid for that particular family of laminates, whereas the ply

interface criterion of Eq. 13 can be applied to any other interface as well. In other words, the traditional failure criteria associated with lamina failures (Hashin) or with out-of-lamina failures (Kim and Soni, Brewer and Lagace, and Lecuyer) represent specific cases of the more general ply interface criterion.

Application of the failure criterion of Eq. 13 to the test data of figure 6, results in the criterion values of figure 10. They have been determined using the local ply failure stresses  $\tau_{13}$  and  $\tau_{23}$  in both plies adjacent to the interface for each specimen, calculated according to paragraph 2.1 and 2.2. The strength values for  $S_{13}$  and  $S_{23}$  are based on the two test configurations with the 0/0 and the 90/90<sup>2</sup> interface. Once again, the average strength values are used, respectively 100.3 MPa and 83.4 MPa.

Comparison of figure 10 with figure 8 seems to suggest that the newly developed failure criterion indeed gives a better prediction of the strength of all the different interfaces. This becomes apparent especially for the 0/90 and 0/45 interfaces (configuration 2 and 3) where the largest differences between the two criteria are to be expected. Whereas the traditional criterion of Eq. 7 results in an overly conservative strength prediction (criterion values exceeding 1.0), the ply interface criterion of Eq. 13 finds values closer to 1.0. In the next chapter statistical proof will be given that the new failure criterion is a better representation of the actual failure behaviour.

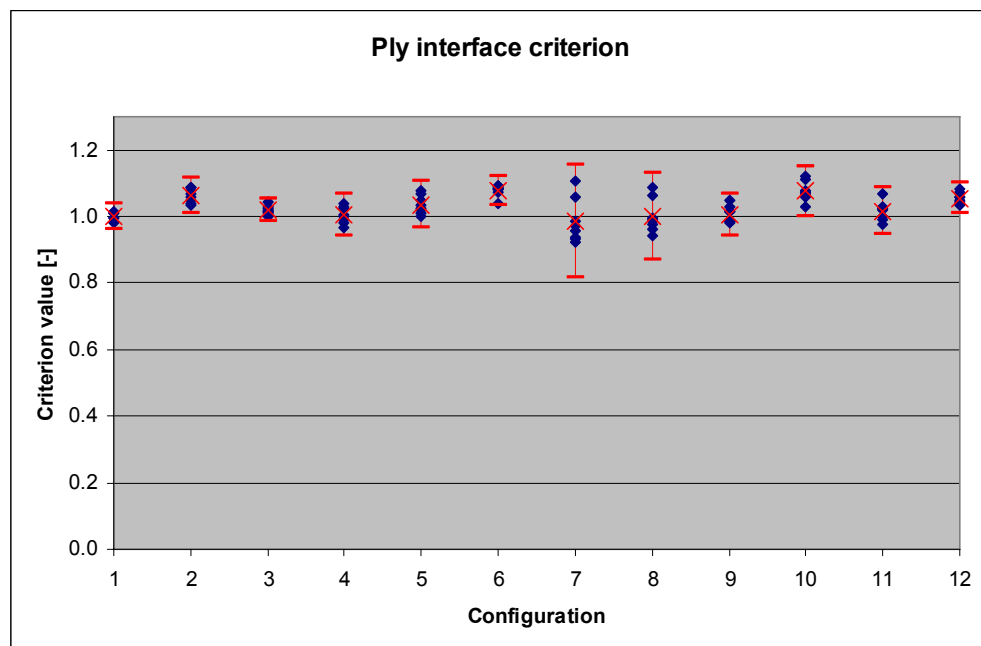


Fig. 10 Value of the failure criterion using the mean strengths of the 0/0 and 90/90<sup>2</sup> interface



### **3 Evaluation of failure criteria using statistical analysis**

In this chapter a statistical analysis procedure is employed to evaluate the traditional and the newly developed criterion of paragraph 2.3. First, some general background information is given on statistical analysis techniques. These techniques are applied to the test data to investigate whether different interfaces indeed show different strength values or if this is nothing more than scatter in the test results. Finally, a procedure is developed for the evaluation of different failure criteria using statistical analysis.

#### **3.1 General background of statistical analysis**

Statistical analysis can help to decide whether observed differences between test data sets are “real” or due to data scatter. Analysis of variance (ANOVA) gives a statistical test of whether the means of several groups are all equal. The test does not tell which group(s) are different from the others...just that there is a difference. “Post-hoc” (after the fact) tests have to be used to examine which groups differ from each other. There is a wide variety of post-hoc tests, but the most common is to do an F-test and/or T-test. Both are statistical hypothesis tests.

A statistical hypothesis test is a method of making statistical decisions using experimental data. These decisions are made using null-hypothesis tests; it answers the question:

*Assuming that the null hypothesis is true, what is the probability of observing a value for the test statistic that is at least as extreme as the value that was actually observed?*

If the probability of observing a value that was actually observed is very low (below a certain critical confidence level) this causes the null hypothesis to be rejected in favour of the alternative hypothesis. So, statistical hypothesis testing is used to make a decision about whether the data contradicts the null hypothesis: this is called significance testing. A null-hypothesis is never proven by such methods, as the absence of evidence against the null-hypothesis does not establish it. In other words, one may either reject, or not reject the null-hypothesis; one cannot accept it. Failing to reject it still allows for the possibility of obtaining further data and then re-examining the same hypothesis.

Below, the F-test and T-test are discussed. The F-test is used to determine whether two experimental data sets have different variances. The T-test is used to determine whether two experimental data sets have different means.

### The F-test

An F-test is used to investigate the hypothesis that the standard deviations of two normally distributed populations are equal, and thus that they are of comparable origin. It is used to compare the variances of two populations, see figure 11. The null-hypothesis is formulated as follows:

*Two sets of data (1 and 2), with sample variances  $\sigma_1$  and  $\sigma_2$ , are both part of the same population, so that their population variances are equal,  $\sigma_1 = \sigma_2$ .*

If we accept this hypothesis, we are saying that despite the fact that the samples came from two different measurements, they are part of the same overall population. If we reject the hypothesis, we are saying the population variances are different, and that we are dealing with two separate populations or sets of data.

The F-test returns the probability that the variances in data sets 1 and 2 are not significantly different. Below a certain confidence level (often  $P < 5\%$ ) the hypothesis is rejected; the population variances are not equal, so the two sets of data are not part of the same population. Please remember, that a confidence level  $P > 5\%$  does not prove that the sample variances are equal, just that there is not enough proof to reject the null-hypothesis.

Note that in testing equality of variances, the F-test is extremely non-robust to non-normality. That is, even if the data displays only modest deviation from the normal distribution, the test is unreliable and should not be used.

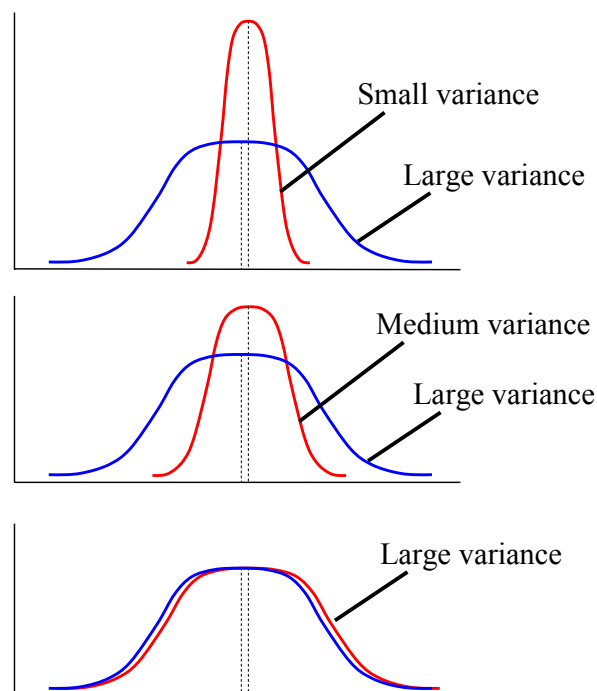


Fig. 11 Three scenario's for differences between variances

### The T-test

A T-test is used to investigate the hypothesis that the means of two normally distributed populations are equal, and thus that they are of comparable origin. It is used to compare the means of two populations, see figure 12. The null-hypothesis is formulated as follows:

*Two sets of data (1 and 2), with sample means  $\mu_1$  and  $\mu_2$ , are both part of the same population, so that their populations means are equal,  $\mu_1 = \mu_2$ .*

If we accept this hypothesis, we are saying that despite the fact that the samples came from two different measurements, they are part of the same overall population. If we reject the hypothesis, we are saying the population means are different, and that we are dealing with two separate populations or sets of data.

The T-test returns the probability that the means in data sets 1 and 2 are not significantly different. Below a certain confidence level (often  $P < 5\%$ ) the hypothesis is rejected; the population means are not equal, so the two sets of data are not part of the same population. Please remember, that a confidence level  $P > 5\%$  does not prove that the sample means are equal, just that there is not enough proof to reject the null-hypothesis.

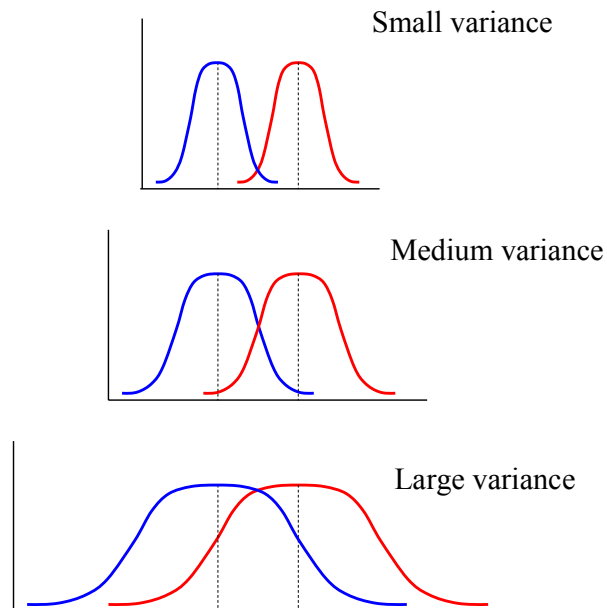


Fig. 12 Three scenario's for differences between means

As an example, consider the three situations shown in figure 12. Notice that the difference between the means is the same in all three situations. However, the three situations give the impression of being very different. The top example shows a case with low variability within

each group. The second situation shows the moderate variability case. The third shows the case with high variability. Clearly, the two groups appear most different or distinct in the low-variability case, because there is relatively little overlap between the two bell-shaped curves. In the high variability case, the group difference appears least striking because the two bell-shaped distributions overlap so much. This leads us to the following conclusion: when looking at the differences between scores for two groups, one should judge the difference between their means relative to their variability. The T-test does just this.

### 3.2 Evaluation of test results

Figure 6 shows the failure stress of all the different configurations. Each configuration has its own mean value and variance. This distribution can be represented by, for instance, a bell-shaped curve. However, there are several different formulas to describe the shape of this curve. The most well-known shapes are the “Normal”, “LogNormal” and “Weibull” distributions. Alternatives are “Cauchy”, “Gumbel”, “Laplace”, and there are many others.

At NLR the software programme RAP++ has been developed, see reference 6. The programme can be used to fit all the different distributions through the test data and find the one with the best fit. It turns out that only the “Normal” and “LogNormal” distribution is able to represent the data scatter or variance for all configurations. Figure 13 shows the best fit for a normal distribution through the test data for the 0/90 interface. The probability plot shows that the normal distribution is very accurate (see reference 6 for a more elaborate discussion on Probability Plots, Probability Density Functions and Cumulative Density Functions). In all further analyses the normal distribution is used, because it is an accurate representation of the test variance and because it is also the assumed distribution when performing an F-test.

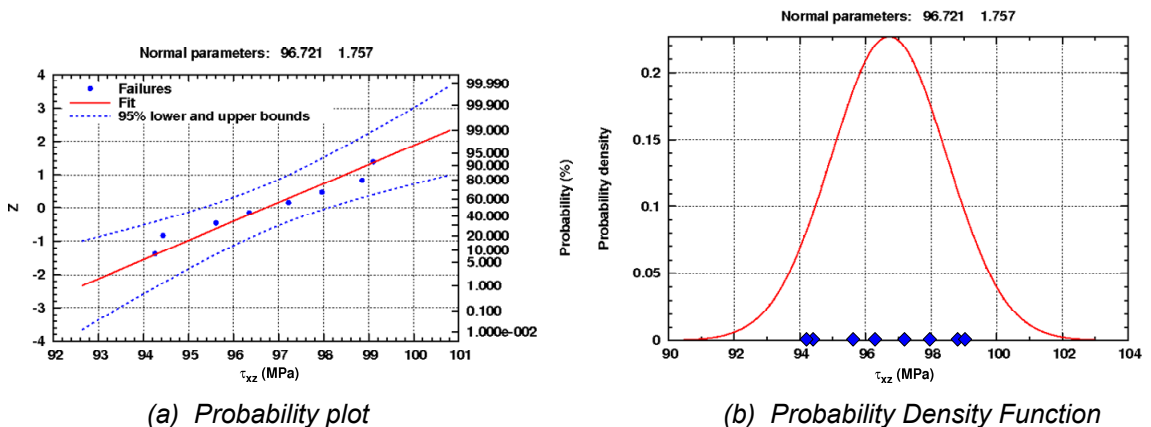


Fig. 13 Normal distribution fitted through the test data for the 0/90 interface (config 2)

The statistical analysis techniques of paragraph 3.1 are applied to the test data in order to investigate whether different interfaces indeed show different strength values or if this is nothing more than scatter in the test results. Of special interest are the four configurations with the 90/θ interfaces, because these result in a clear difference between the strength predictions according to traditional criteria and the newly developed ply interface criterion. The traditional “single ply” criterion predicts identical strengths for all configurations with the 90° ply being the critical ply in all configurations. Contrary, the ply interface criterion predicts different strengths for different interfaces.

Figure 14 shows the failure stress  $\tau_{xz}$  for the specimens of the four 90/θ configurations. In figure 15 a normal distribution has been fitted through the test data for each configuration. This already offers better insight in the differences between the four configurations. Based on these two figures, one would probably regard configuration 7 and 8 as the same, whereas configurations 2 and 4 would be regarded as different sets of data.

Next, the F- and T-tests are applied to the test data to quantify this impression. The F-test is used to determine whether the assumption of equal variances for two sets of data should be rejected or not. If not, a T-test (assuming equal variances) is applied to determine whether the assumption of equal means should be rejected or not. For both tests a critical confidence level of 5 % is taken. When the probability is below 5 % the hypothesis of equal variances/means is rejected. A two-way comparison is made in which all of the data sets are compared separately with each other. The minimum confidence level of both tests is given in table 2. It can be seen that in this case, the initial feeling is supported by the significance testing. There is only a very small probability that the test results for the 0/90 and 45/90 interfaces are the same as for any of the other configurations. In other words, it is very likely that different sets of data have been found, each with their own strength values. The only two data sets, for which the null-hypothesis of equal variances and equal means may not be rejected, are the two configurations with the 90/90 interface. Of course, one would expect to find similar failure stresses because the strength is dictated by the same critical interface.

The above shows how statistical analyses can be used to interpret the test results. Statistical analysis points out distinct differences for the strength of 0/90, 45/90 and 90/90 interfaces. For a correct representation of the failure behaviour, this should of course be captured by the failure criterion. However, this is not the case for the traditional “single ply” criteria presented in paragraph 2.3.1.

The results also show that it is not necessary to place a 45° ply in between the outer 0° plies and the inner 90° plies of the ILS specimens to ensure a proper failure location (the 90/90 interface), because similar strength values have been found for both configurations. In fact, it is even better to leave out the 45° ply. The test results of figure 6 show that the strength of the 45/90 interface

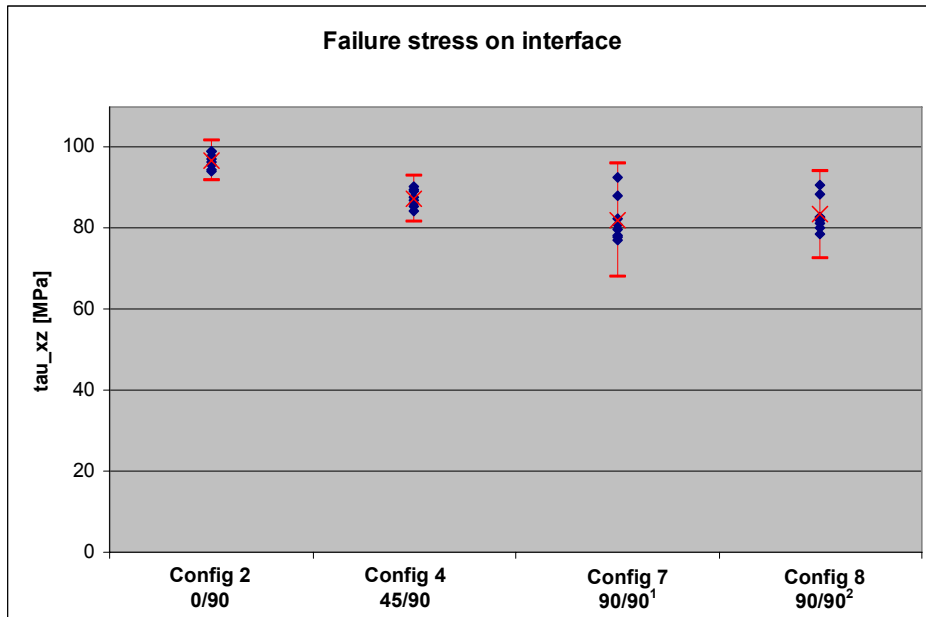


Fig. 14 ILS failure stresses for the 90/θ interfaces

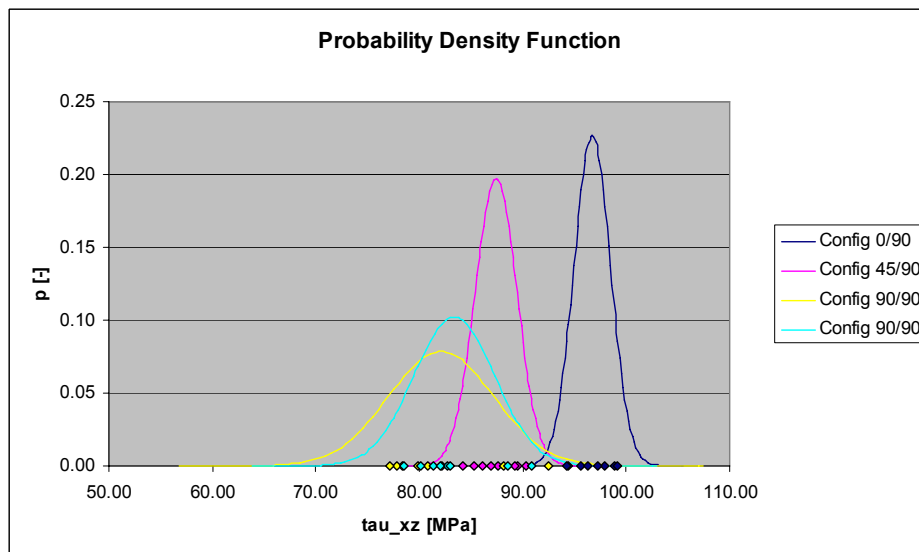


Fig. 15 ILS strength distributions (PDF) for the 90/θ interfaces

Table 2 Significance level that the observed differences are due to chance (90/θ interfaces), i.e. probability that the variances and means of two data sets are equal

	0/90	45/90	90/90 <sup>1</sup>	90/90 <sup>2</sup>
0/90	100%	0.0%	0.0%	0.0%
45/90		100%	2.2%	3.0%
90/90 <sup>1</sup>			100%	50.9%
90/90 <sup>2</sup>				100%



**Table 3** Significance level that the observed differences are due to chance (all interfaces), i.e. probability that the variances and means of two data sets are equal

	0/0	0/90	0/45	45/90	45/45	45/-45	90/90 <sup>1</sup>	90/90 <sup>2</sup>	30/-30	60/-60	30/30	60/60
0/0	100%	0.2%	0.1%	0.0%	0.0%	1.7%	0.0%	0.0%	0.2%	0.0%	1.0%	0.0%
0/90		100%	31.3%	0.0%	2.8%	11.2%	0.0%	0.0%	55.7%	1.8%	40.7%	0.0%
0/45			100%	0.0%	0.5%	24.7%	0.0%	0.0%	12.5%	0.3%	7.4%	0.0%
45/90				100%	0.0%	0.0%	2.2%	3.0%	0.0%	0.0%	0.0%	0.1%
45/45					100%	0.1%	0.0%	0.0%	10.7%	83.3%	4.6%	3.6%
45/-45						100%	0.0%	0.0%	5.3%	0.1%	19.0%	0.0%
90/90 <sup>1</sup>							100%	50.9%	0.0%	0.0%	0.0%	0.0%
90/90 <sup>2</sup>								100%	0.0%	0.0%	0.0%	0.0%
30/-30									100%	0.0%	0.0%	0.0%
60/-60										100%	7.3%	57.5%
30/30											100%	3.2%
60/60												100%

is smaller than the strength of the 0/90 interface, so interleaving a 45° ply actually increases the chance of failure at the wrong interface.

For the sake of completeness, the significance level has been determined for all configurations. This is shown in table 3. It can be seen that in most cases the assumption of equal variances and equal means has to be rejected, indicating different strength values for different interfaces. Please remember, that a confidence level  $P > 5\%$  does not prove that identical sets of data have been found, just that there is not enough proof to reject the null-hypothesis of equal variances and equal means. There is still the possibility of obtaining further data (e.g. by testing more samples or by application of other load cases) and then re-examining the same hypothesis.

### 3.3 Evaluation of failure criteria

The previous paragraph already gives ample reason not to use the traditional “single ply” criteria of paragraph 2.3.1. These criteria cannot explain all the different strengths observed in tests. This is taken care of in the out-of-lamina criteria by limiting their validity to a certain “family of laminates”, but this of course makes them unsuitable for general application. Although the newly developed ply interface criterion of paragraph 2.3.2 is able to predict different strength values for different interfaces and seems to perform better (compare Fig. 8 to Fig. 10), this does not prove yet that it really is a better representation of the interface strength. Therefore, a procedure has been developed to rank/evaluate failure criteria. This is discussed below.

#### 3.3.1 Statistical procedure

The here-presented method or procedure for evaluation of failure criteria is suitable for general application. Any criterion can be checked with this particular procedure. All criteria need test results as input. This can be either strength data or strain data. In the case of the two criteria evaluated here (Eq. 7 and Eq. 13), it is strength data for  $S_{13}$  and  $S_{23}$ . These are the strengths of the 0/0 interface and the 90/90 interface and are generated by tests on the

**Step 1:** Find best fit for strength distribution of  $S_{13}$  on 0/0 specimens and  $S_{23}$  on 90/90 specimens

**Step 2:** Use  $S_{13}$  and  $S_{23}$  probability distribution and failure criterion in Monte-Carlo-Simulation to predict strength distribution for all other configurations

**Step 3:** Compare predicted strength distribution with actual failures from test

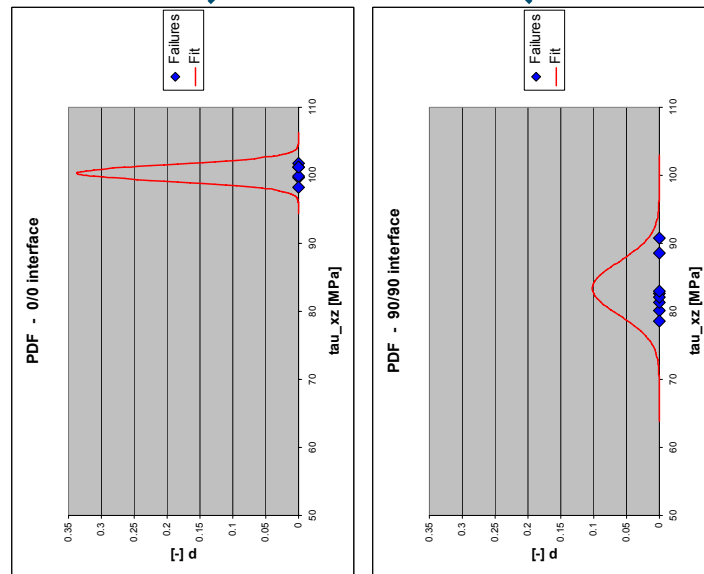


Fig. 16 Statistical procedure for evaluation of failure criteria



appropriate specimen configuration. The evaluation procedure starts with fitting a probability density function on these test results; step 1 in figure 16. Different distributions are found for the required strength input data.

This curve with the “best fit” for the strength distribution and a certain failure criterion are used in a Monte-Carlo-Simulation to predict the strength of all other configurations and loading conditions; step 2 in figure 16. Different criteria will of course result in different predictions. Usually the criteria need some reworking as well. In this case, the maximum shear stress in global laminate direction  $\tau_{xz}$  on the critical interface has to be determined for each configuration. For the “single ply” criterion of paragraph 2.3.1 this becomes:

$$\tau_{xz} = \min \left\{ \left( \frac{\cos^2 \theta_1}{S_{13}^2} + \frac{\sin^2 \theta_1}{S_{23}^2} \right)^{\frac{1}{2}} ; \left( \frac{\cos^2 \theta_2}{S_{13}^2} + \frac{\sin^2 \theta_2}{S_{23}^2} \right)^{\frac{1}{2}} \right\} \quad \text{Eq. 14}$$

For the ply interface criterion of paragraph 2.3.2 one can derive:

$$\tau_{xz} = \left( \frac{\cos^2 \theta_1 + 2 \cdot \cos \theta_1 \cdot \cos \theta_2 \cdot \cos(\theta_1 - \theta_2) + \cos^2 \theta_2}{4 \cdot S_{13}^2} + \frac{\sin^2(\theta_1 - \theta_2)}{2 \cdot S_{13} \cdot S_{23}} + \frac{\sin^2 \theta_1 + 2 \cdot \sin \theta_1 \cdot \sin \theta_2 \cdot \cos(\theta_1 - \theta_2) + \sin^2 \theta_2}{4 \cdot S_{23}^2} \right)^{\frac{1}{2}} \quad \text{Eq. 15}$$

So, with Eq. 14 and Eq. 15 and with the two probability density functions for  $S_{13}$  and  $S_{23}$  a new strength distribution can be predicted for every other configuration, because this only depends now on the ply angles  $\theta_1$  and  $\theta_2$  of the two plies adjacent to the interface. The Monte Carlo Simulation calculates these new strength distributions or probability density functions for all other configurations.

Finally, the predicted strength (which is an entire distribution function) can be compared with the actual failures found by test; step 3 in figure 16. Of course the F-test and T-test can be used to calculate the confidence level for the assumption of equal means and variances. If the confidence level or probability is too small (below 5 %) the prediction is not accurate enough and the failure criterion is not successful in predicting the correct strength of the interface.

The most important assumption in the above-outlined approach is that both variance and mean value should be predicted accurately by the failure criterion in order to correctly describe the failure behaviour. This implies that the predicted relation between the distributions of test results for different configurations, is assumed to exist in reality as well!!



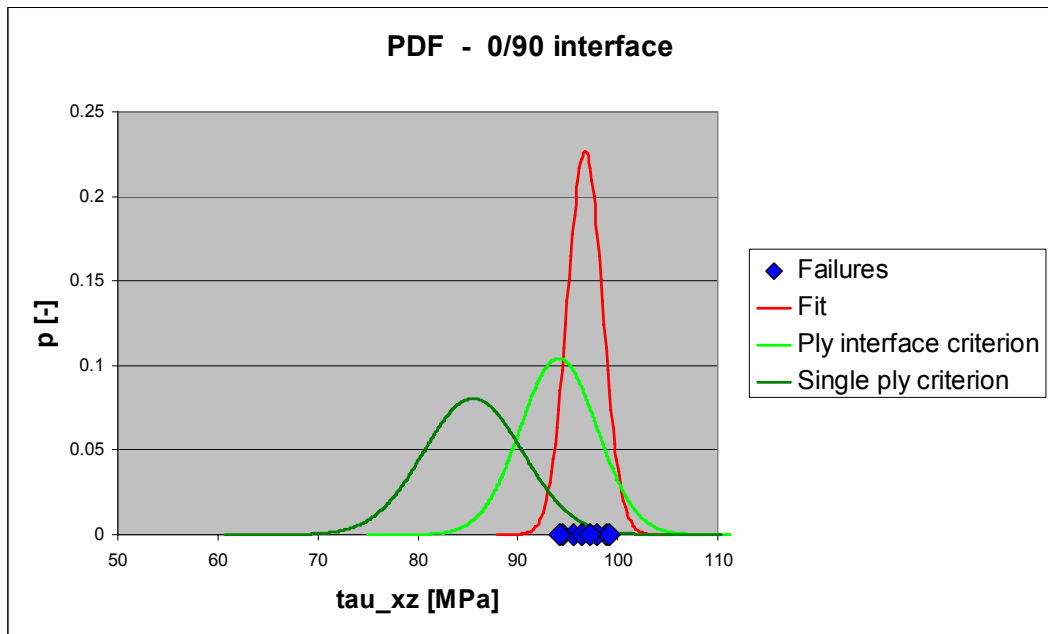
### 3.3.2 Evaluation of ILS failure criteria

Figure 17 gives the results after application of the statistical procedure of the previous paragraph to the 0/90 and 0/45 configurations. The dark green line gives the predicted probability density function according to the “single ply” criterion (Eq. 7 and Eq. 14). The light green line gives the predicted probability density function in accordance with the ply interface criterion (Eq. 13 and Eq. 15). The blue diamonds are actual failures found by test on that particular interface, for which the fitted normal distribution is shown as well (the red line). For comparison between prediction and test results with the F- and T-test, not the fitted distribution is used but the (limited amount of) actual test points.

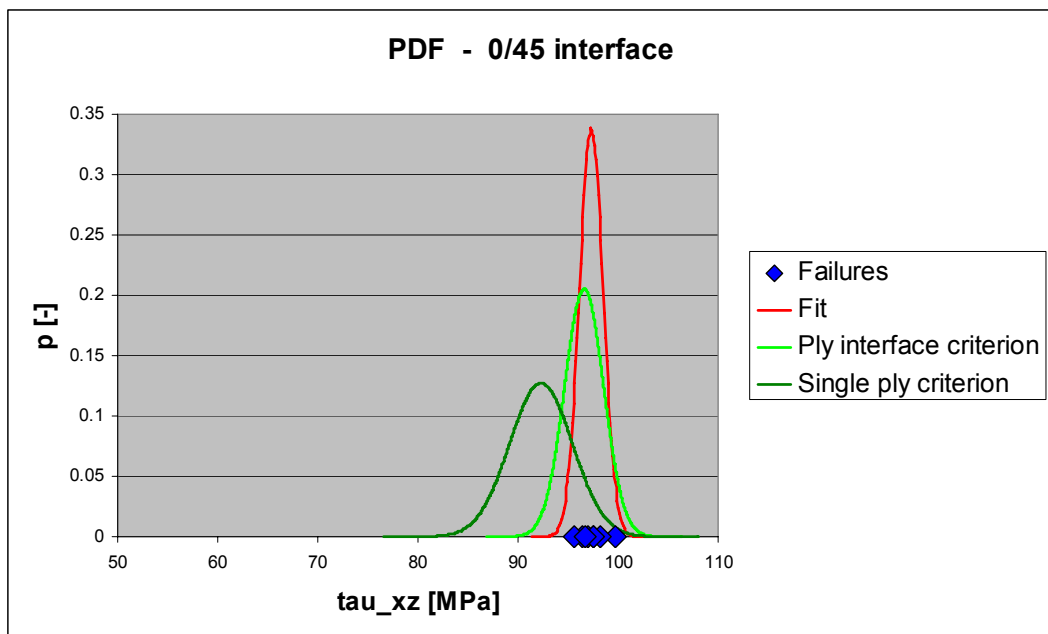
It can be seen in figure 17 that for the 0/90 and 0/45 interface the strength prediction of the ply interface criterion resembles the test data better than the “single ply” criterion. This is confirmed by the F- and T-test. Whereas the probability of equal variances and equal means cannot be rejected for the ply interface criterion ( $P > 5\%$ ), both the variances and the means are regarded as unequal for the prediction with the “single ply” criterion; the probability for equal variances is only 1.1 % and 1.5 % for the 0/90 and 0/45 interface, and the probability for equal means is 0.0 % for both interfaces. This is summarised in table 4 with the simple statements “Equal/Unequal variances” and “Equal/Unequal means”.

Table 4 Application of F-test and T-test to compare test data with strength predictions

Config	Ply interface criterion	Single ply criterion
0/0	Equal variances Equal means	Equal variances Equal means
0/90	Equal variances Equal means	Unequal variances Unequal means
0/45	Equal variances Equal means	Unequal variances Unequal means
45/90	Equal variances Equal means	Equal variances Equal means
45/45	Equal variances Equal means	Equal variances Equal means
45/-45	Equal variances Unequal means	Equal variances Unequal means
90/90 <sup>1</sup>	Equal variances Equal means	Equal variances Equal means
90/90 <sup>2</sup>	Equal variances Equal means	Equal variances Equal means
30/-30	Equal variances Equal means	Equal variances Equal means
60/-60	Equal variances Equal means	Equal variances Equal means
30/30	Equal variances Equal means	Equal variances Equal means
60/60	Unequal variances Equal means	Unequal variances Equal means



(a) Probability density functions for the strength of 0/90 interface



(b) Probability density functions for the strength of 0/45 interface

Fig. 17 Test results compared to strength predictions using the procedure of paragraph 3.3.1

Table 4 shows the results for all other configurations as well. It can be seen that for the two investigated criteria the only differences are found for the 0/90 and 0/45 interface, already shown in figure 17. Please notice, that this does not mean that there are no differences whatsoever for the two predictions, just that both predictions are ranked/classified the same by the F- and T-test. This is shown in figure 18 for the 45/90 interface. Especially the mean value differs for the two predictions. However, although the mean value predicted by the ply interface criterion is closer to the actual test results (1.7 % difference) than the mean value predicted by the “single ply” criterion (2.6 % difference), the null hypothesis of equal means and variances cannot be rejected yet for neither one of the criteria. Of course it is still possible to obtain more test data by which one or even both predictions may be classified as unequal.

Based on the formulation of the two criteria, Eq. 7 and Eq. 14 compared to Eq. 13 and Eq. 15, the largest differences would indeed be expected for the configurations with the 0/90, 0/45 and 45/90 interface. All other configurations result in exactly the same prediction (for the  $\theta/\theta$  interfaces) or only very small differences (for the  $\theta/-\theta$  interfaces). When performing an F- and T-test on these predictions both criteria will be ranked the same.

Finally, it can be seen in table 4 that with the ply interface criterion only for the 45/-45 interface and the 60/60 interface distinct differences are found between prediction and test. The probability density functions are shown in figure 19. For the 45/-45 different means are found. Both criteria underestimate the strength of the interface, the ply interface criterion with 5.6 % and the “single ply” criterion with 6.0 %. For the 60/60 interface different variances are found. Both criteria overestimate the amount of variance or data scatter.

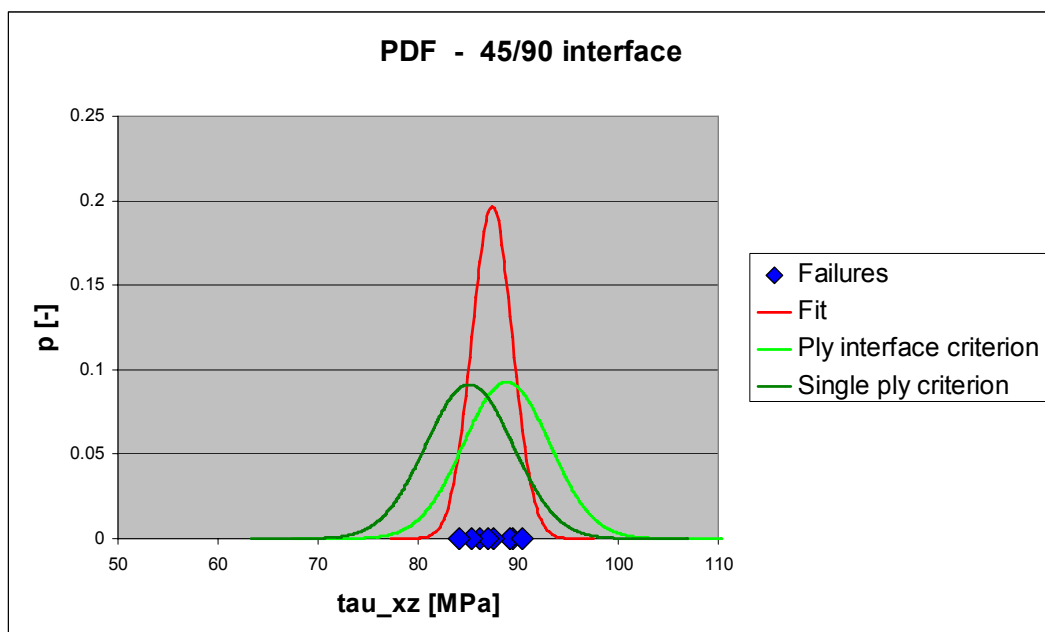
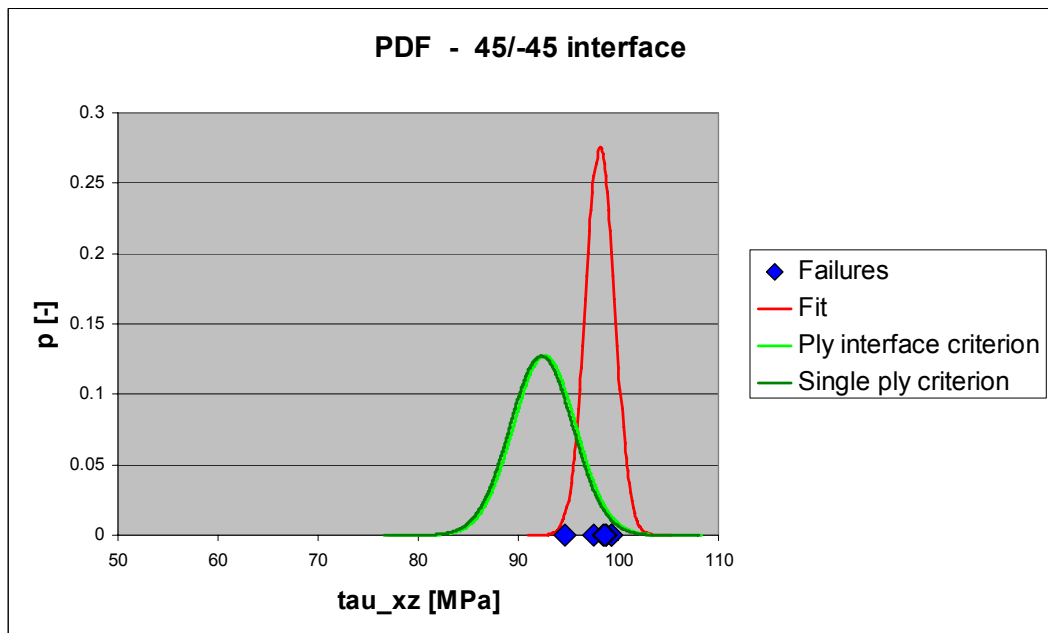
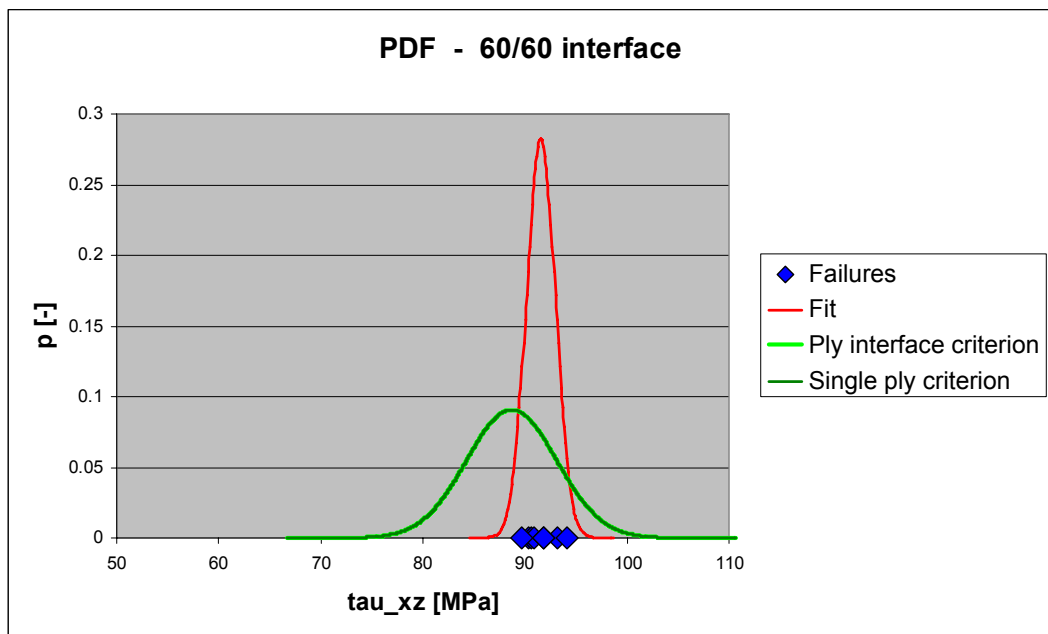


Fig. 18 Probability density functions (prediction and test) for the strength of 45/90 interface



(a) Probability density functions for the strength of 45/-45 interface



(b) Probability density functions for the strength of 60/60 interface

Fig. 19 Test results compared to strength predictions using the procedure of paragraph 3.3.1

## 4 Conclusions and recommendations

The test results on thin ILS coupons showed distinct differences for the strength of different interfaces. This was confirmed by statistical analysis of these test results. Not all differences in strength could be explained by traditional ILS criteria, such as Hashin and Kim&Soni. Therefore, a new “ply interface” criterion has been formulated for the Interlaminar Shear strength of the interface between two plies:

$$\frac{\tau_{13,\text{ply}1}^2 + 2 \cdot \tau_{13,\text{ply}1} \cdot \tau_{13,\text{ply}2} \cdot \cos(\theta_1 - \theta_2) + \tau_{13,\text{ply}2}^2}{4 \cdot S_{13}^2} + \frac{(\tau_{13,\text{ply}1} \cdot \tau_{23,\text{ply}2} - \tau_{13,\text{ply}2} \cdot \tau_{23,\text{ply}1}) \cdot \sin(\theta_1 - \theta_2)}{2 \cdot S_{13} \cdot S_{23}} + \frac{\tau_{23,\text{ply}1}^2 + 2 \cdot \tau_{23,\text{ply}1} \cdot \tau_{23,\text{ply}2} \cdot \cos(\theta_1 - \theta_2) + \tau_{23,\text{ply}2}^2}{4 \cdot S_{23}^2} \leq 1$$

The ILS strength of any arbitrary interface can be calculated based on:

- The local ply stresses in both plies adjacent to the interface
- The difference in ply angles between the two plies
- The two shear strength values  $S_{13}$  and  $S_{23}$  of the 0/0 and 90/90 interface.

The strength of the 0/0 interface and 90/90 interface can be determined by tests on  $[0_m]_S$  and  $[0_n, 90]_S$  coupons. The thickness (which) defines the number of plies can be chosen similar to the ASTM standard of Ref. 7, but should in any case be large enough to prevent bending failures. So, when setting up test programmes in the future, both configurations should be manufactured and tested.

Next to a new failure criterion, a statistical method has been developed to evaluate different failure criteria. It is suitable for general application, so any criterion can be checked with this particular procedure. The basic assumption of this method is that in order to correctly describe the failure behaviour both variance and mean value should be predicted accurately by the criterion. This implies that there is a relation between the distributions or data scatter for different configurations, which actually exist in reality and is captured correctly by the criterion. Application of this procedure to the newly developed ply interface criterion and traditional criteria, which consider stresses in one ply only, shows that the new criterion indeed performs better, which was already suspected during the NIVR-SRP programme of Ref. 1. This is especially the case for the 0/90 and 0/45 interfaces, or more generally for configurations with highly dissimilar ply stresses in the two plies adjacent to the interface. Looking at the formulation of the new and traditional criterion this is exactly where the largest differences are to be expected.

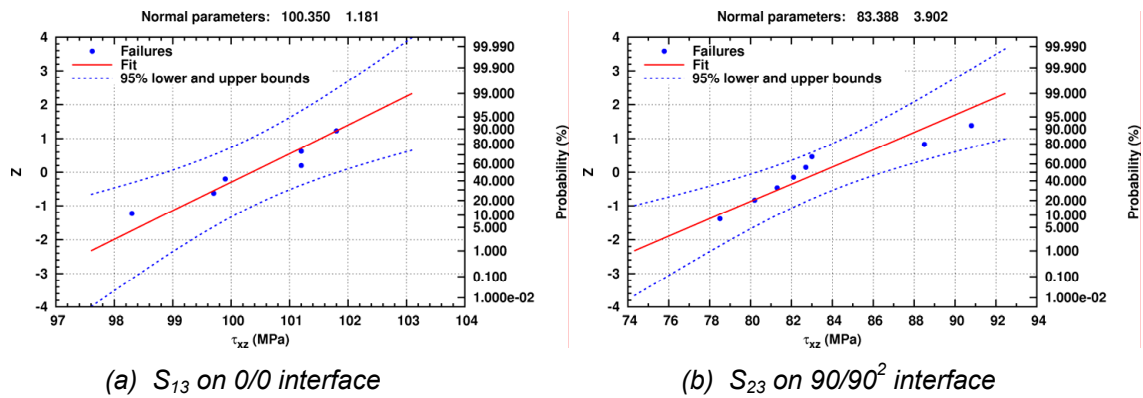


Fig. 20 Probability plot including confidence bounds

It is noted here, that the current statistical procedure for evaluation of failure criteria is performed with “exact” distributions for  $S_{13}$  and  $S_{23}$ . A probability density function is fitted through the (limited amount of) test data points. The two fitted curves are used as input in the Monte Carlo Simulation to predict the strength distribution of all other configurations. However, the distributions for  $S_{13}$  and  $S_{23}$  are based on relatively small sample sizes, so there is some uncertainty in the fitted curves. This can be visualised in the probability plots for both test configurations. Figure 20 shows that there is still some uncertainty in the fitted curve, which is represented by the 95 % confidence bounds. It is hard to visualise this uncertainty in the probability density functions as shown in figure 16, but it should be included somehow in the Monte Carlo Simulation. Alternatively, more samples could be tested to narrow down the confidence bounds in figure 20. Testing more samples usually has more influence on the variance than on the mean value, but the amount of data scatter influences the outcome of both the F- and T-test.

Another improvement of the accuracy of the analysis is the application of the Finite Element Method (FEM) to determine the ply stresses. Currently, these stresses are based on CPT, see paragraph 2.1. In the previously mentioned NIVR-SRP programme of Ref. 1, it was shown that CPT is only valid at a certain distance from the load introduction points. Therefore, in the future FEM interface elements should be equipped with the ply interface criterion. This is not so straightforward, because these elements need information (at least the ply angle) from other elements to which they are attached. Further, a damage law should be included in order to determine not only initial cracking but also the final failure load, in case there is any difference at all.

As a last remark, it is noted here that further research is necessary towards the influence of other stress components (e.g.  $\sigma_3$ ). This has been the subject of many other research programmes and it is generally believed that transverse tensile stresses promote the formation of interlaminar shear cracks, while transverse compressive stresses postpone the cracking.

## References

1. Creemers, R.J.C.; *NIVR-SRP Proposal on "Transverse Load Introduction in Thick Composite Aircraft Structures"*, NLR-Memorandum AVST-2006-080, National Aerospace Laboratory NLR, Amsterdam, 2006.
2. Creemers, R.J.C.; Nijhuis, P.; Wilson, W.; Smeets, M.; *Transverse loads in thick composite structures - a literature research*, NLR-CR-2007-533, National Aerospace Laboratory NLR, Amsterdam, 2007.
3. ASTM D2344-00, *Standard Test Method for Short-Beam Strength of Polymer Matrix Composite Materials and Their Laminates*.
4. Timoshenko S.; Woinowsky-Krieger S.; *Theory of plates and shells*, McGraw-Hill Book Company, Inc., 1959.
5. Rohwer K.; Friedrichs S.; Wehmeyer C.; *Analyzing Laminated Structures from Fibre-Reinforced Composite Material - An Assessment*, Technische Mechanik, Band 25, 2005.
6. Grooteman, F.P.; *Reliability Analysis Program for design of structures - RAP++ User Manual v2.0.5*, NLR-TR-2007-007, National Aerospace Laboratory NLR, Amsterdam, 2007.
7. ASTM D2344-00, *Standard Test Method for Short-Beam Strength of Polymer Matrix Composite Materials and Their Laminates*.



## Appendix A The analytical determination of transverse shear stresses

### A.1 The basic equations for Classical Plate Theory

#### Force equilibrium

Consider a plate in the (x,y)-plane and assume that all loads are normal to its surface.

Figure A-1 shows a plate under lateral loading. If the deflections are small in comparison with the thickness of the plate, according to Ref. 4, the following equations can be obtained.

Equilibrium of forces on the plate gives:

$$\frac{\partial Q_x}{\partial x} + \frac{\partial Q_y}{\partial y} + p = 0 \quad \text{Eq. A-1}$$

Equilibrium of moments on the plate gives:

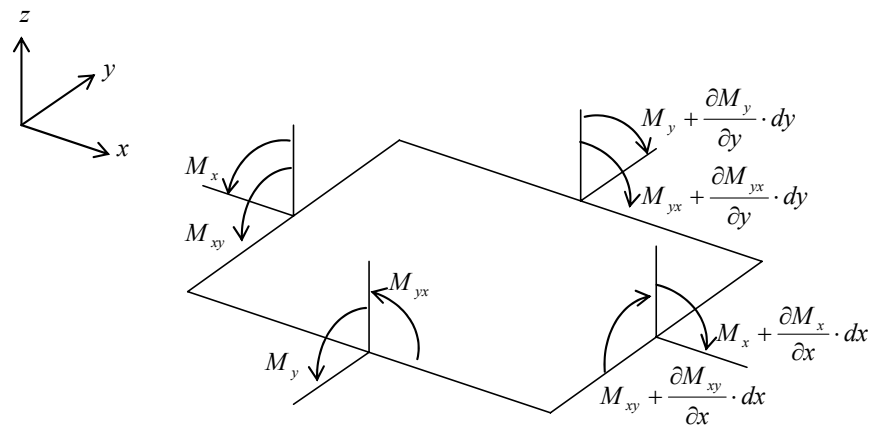
$$\frac{\partial M_{xy}}{\partial x} + \frac{\partial M_y}{\partial y} - Q_y = 0$$

$$\frac{\partial M_{yx}}{\partial y} + \frac{\partial M_x}{\partial x} - Q_x = 0 \quad \text{Eq. A-2}$$

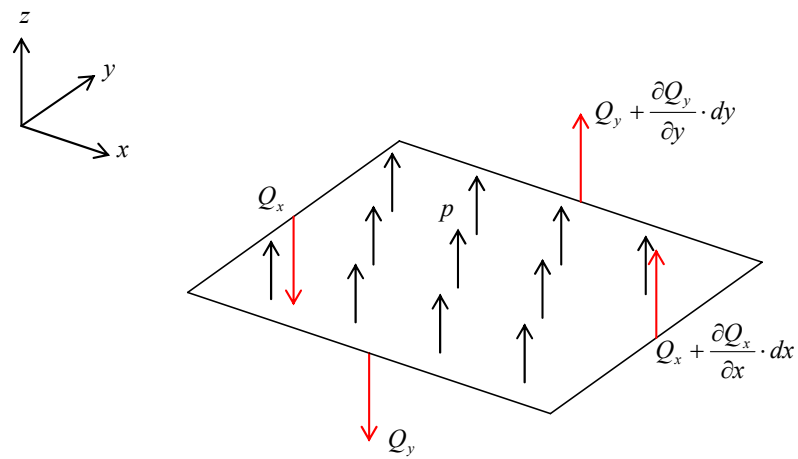
When only forces in the x-direction are considered without gradients the y-direction ( $Q_y = 0$  and  $\partial/\partial y = 0$  for all response variables) this reduces to the following two equations:

$$\frac{\partial Q_x}{\partial x} = -p$$

$$\frac{\partial M_x}{\partial x} = Q_x \quad \text{Eq. A-3}$$



(a) Bending and twisting moments



(b) Vertical shearing forces

Fig. A-1 Plate under lateral loading

The forces and moments acting on the plate cause internal stresses. Now consider an element with dimensions  $dx$ ,  $dy$ ,  $dz$ , see figure A-2. According to Ref. 5 the equilibrium of forces gives the following equations:

$$\begin{aligned}\frac{\partial \sigma_x}{\partial x} + \frac{\partial \tau_{xy}}{\partial y} + \frac{\partial \tau_{xz}}{\partial z} &= 0 \\ \frac{\partial \tau_{yx}}{\partial x} + \frac{\partial \sigma_y}{\partial y} + \frac{\partial \tau_{yz}}{\partial z} &= 0 \\ \frac{\partial \tau_{zx}}{\partial x} + \frac{\partial \tau_{zy}}{\partial y} + \frac{\partial \sigma_z}{\partial z} &= 0\end{aligned}\tag{Eq. A-4}$$

Equilibrium of moments, neglecting the higher order terms, results in:

$$\begin{aligned}\tau_{xy} &= \tau_{yx} \\ \tau_{yz} &= \tau_{zy} \\ \tau_{zx} &= \tau_{xz}\end{aligned}\tag{Eq. A-5}$$

When only stress gradients in the y-direction are considered ( $\partial/\partial y = 0$  for all response variables) and the last three equations are substituted in the first three, this reduces to the following three equations:

$$\begin{aligned}\frac{\partial \sigma_x}{\partial x} + \frac{\partial \tau_{xz}}{\partial z} &= 0 \\ \frac{\partial \tau_{xy}}{\partial x} + \frac{\partial \tau_{yz}}{\partial z} &= 0 \\ \frac{\partial \tau_{zx}}{\partial x} + \frac{\partial \sigma_z}{\partial z} &= 0\end{aligned}\tag{Eq. A-6}$$

Notice, that a two-dimensional approach would have resulted in the first and last equation only, see figure A-3. However, the second equation shows that, although no stress gradients are considered in y-direction, the stress components in y-direction themselves ( $\tau_{xy}$ ,  $\tau_{yz}$  and also  $\sigma_y$ ) are not necessarily zero as well.

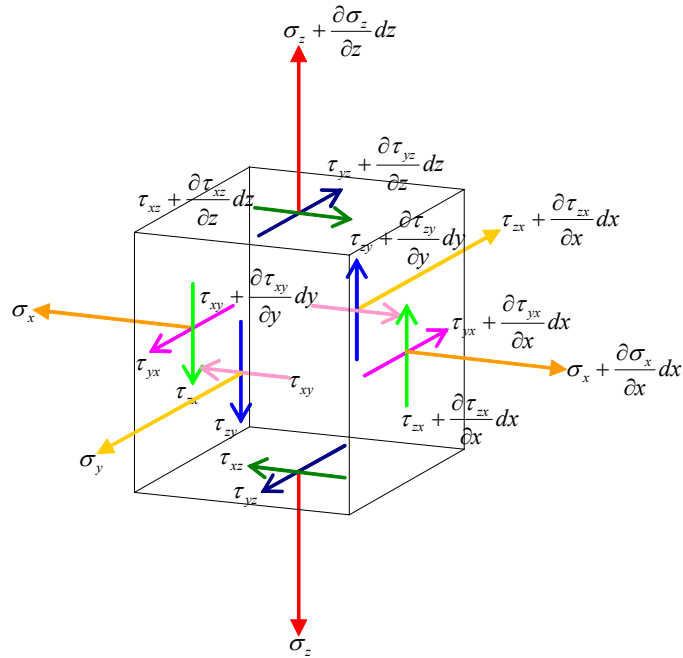


Fig. A-2 Stresses acting on an element with dimensions  $dx$ ,  $dy$ ,  $dz$

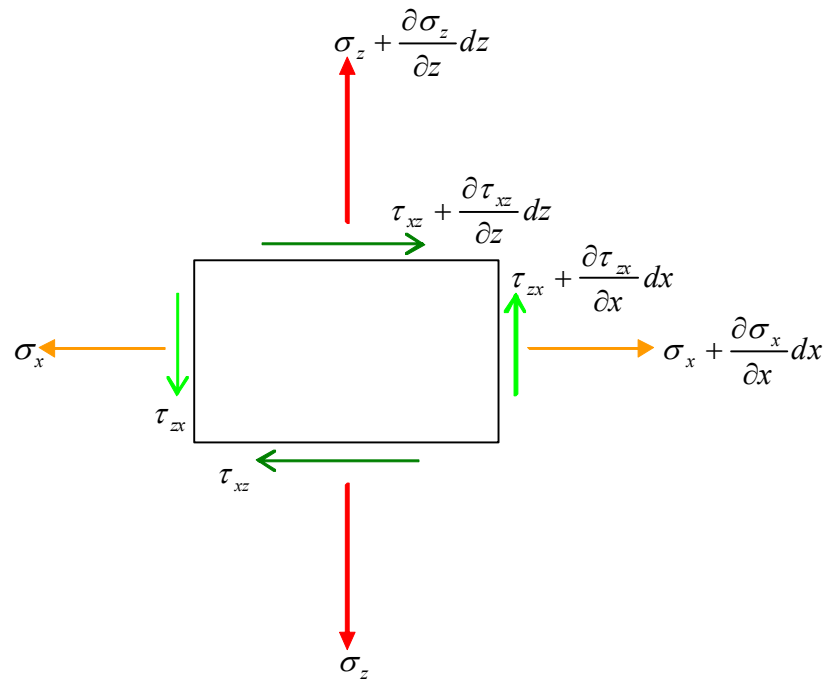


Fig. A-3 Stresses acting on an element with dimensions  $dx$ ,  $dz$ .

### Force resultants

Next, the relation between the loads and the stresses can be established. The magnitude of the shearing forces can be calculated with:

$$Q_x = \int_{-h/2}^{h/2} \tau_{xz} \cdot dz$$

$$Q_y = \int_{-h/2}^{h/2} \tau_{yz} \cdot dz$$
Eq. A-7

As it was assumed that  $Q_y = 0$ , the shear stress  $\tau_{yz}$  integrated over the entire thickness  $h$  has to be zero. Notice that it still does not mean that the shear stress  $\tau_{yz}$  has to be zero at any location through the thickness, only the resultant shear force in the cross-section is zero.

The in-plane loads are calculated with:

$$N_x = \int_{-h/2}^{h/2} \sigma_x \cdot dz$$

$$N_y = \int_{-h/2}^{h/2} \sigma_y \cdot dz$$

$$N_{xy} = \int_{-h/2}^{h/2} \tau_{xy} \cdot dz$$
Eq. A-8

Only loads in x-direction are considered, or  $N_y = N_{xy} = 0$ . Again, it does not mean that  $\sigma_y$  and  $\tau_{xy}$  are zero at any location through the thickness, only that the resultant in the cross-section is zero.

The moments are calculated with:

$$M_x = \int_{-h/2}^{h/2} \sigma_x \cdot z \cdot dz$$

$$M_y = \int_{-h/2}^{h/2} \sigma_y \cdot z \cdot dz$$

$$M_{xy} = \int_{-h/2}^{h/2} \tau_{xy} \cdot z \cdot dz$$
Eq. A-9

Only loads in x-direction are considered, so the resultant moments  $M_y = M_{xy} = 0$ .

### Kinematics

When it is assumed that cross-sections in the plate of figure A-1 remain straight under loading, the total deformation at any point through the thickness can be subdivided into a component due to the deformation of the mid-plane and a component due to bending:

$$\begin{Bmatrix} \varepsilon_x \\ \varepsilon_y \\ \gamma_{xy} \end{Bmatrix} = \begin{Bmatrix} \bar{\varepsilon}_x \\ \bar{\varepsilon}_y \\ \bar{\gamma}_{xy} \end{Bmatrix} + \begin{Bmatrix} \bar{\kappa}_x \\ \bar{\kappa}_y \\ 2 \cdot \bar{\kappa}_{xy} \end{Bmatrix} \cdot z \quad \text{Eq. A-10}$$

### Constitutive equations

Hooke's law gives the relation between stresses and strain:

$$\begin{Bmatrix} \varepsilon_x \\ \varepsilon_y \\ \gamma_{xy} \end{Bmatrix} = \begin{bmatrix} \frac{1}{E_x} & \frac{-\nu_{xy}}{E_x} & 0 \\ & \frac{1}{E_y} & 0 \\ & & \frac{1}{G_{xy}} \end{bmatrix} \cdot \begin{Bmatrix} \sigma_x \\ \sigma_y \\ \tau_{xy} \end{Bmatrix} \quad \text{or} \quad \{\varepsilon\} = [S] \cdot \{\sigma\} \quad \text{Eq. A-11}$$

Actually, this is only valid for a plate in the state of generalised plane stress, which strictly spoken is not true in our case.

Eq. A-11 can be rewritten as:

$$\{\sigma\} = [C] \cdot \{\varepsilon\} \quad \text{Eq. A-12}$$

In which:

$$[C] = [S]^{-1} = \begin{bmatrix} \frac{E_x}{1 - \nu_{xy} \cdot \nu_{yx}} & \frac{\nu_{xy} \cdot E_y}{1 - \nu_{xy} \cdot \nu_{yx}} & 0 \\ & \frac{E_y}{1 - \nu_{xy} \cdot \nu_{yx}} & 0 \\ & & G_{xy} \end{bmatrix}$$

Substitution of Eq. A-10 into Eq. A-12 gives the stresses as function of (mid-plane) strains and curvature.

## A.2 Implementation of CPT for isotropic materials

For isotropic materials the following simplifications can be made:

$$\begin{aligned}
 E_x &= E_y = E \\
 \nu_{xy} &= \nu_{yx} = \nu \\
 G_{xy} &= G = \frac{E}{2 \cdot (1 + \nu)}
 \end{aligned}
 \tag{Eq. A-13}$$

Substitution of Eq. A-10 and Eq. A-13 into Eq. A-12, followed by substitution into Eq. A-8 and integration over the entire height gives:

$$\begin{aligned}
 N_x &= \frac{E \cdot h}{1 - \nu^2} (\bar{\varepsilon}_x + \nu \cdot \bar{\varepsilon}_y) & \bar{\varepsilon}_x &= \frac{N_x}{E \cdot h} \\
 N_y &= \frac{E \cdot h}{1 - \nu^2} (\nu \cdot \bar{\varepsilon}_x + \bar{\varepsilon}_y) = 0 & \bar{\varepsilon}_y &= -\nu \cdot \bar{\varepsilon}_x \\
 N_{xy} &= G \cdot \bar{\gamma}_{xy} \cdot h = 0 & \bar{\gamma}_{xy} &= 0
 \end{aligned}
 \tag{Eq. A-14}$$

Substitution of Eq. A-10 and Eq. A-13 into Eq. A-12, followed by substitution into Eq. A-9 and integration over the entire height gives:

$$\begin{aligned}
 M_x &= \frac{1}{12} \cdot \frac{E \cdot h^3}{1 - \nu^2} (\bar{\kappa}_x + \nu \cdot \bar{\kappa}_y) & \bar{\kappa}_x &= 12 \cdot \frac{M_x}{E \cdot h^3} \\
 M_y &= \frac{1}{12} \cdot \frac{E \cdot h^3}{1 - \nu^2} (\nu \cdot \bar{\kappa}_x + \bar{\kappa}_y) = 0 & \bar{\kappa}_y &= -\nu \cdot \bar{\kappa}_x \\
 M_{xy} &= \frac{1}{6} \cdot G \cdot \bar{\kappa}_{xy} \cdot h^3 = 0 & \bar{\kappa}_{xy} &= 0
 \end{aligned}
 \tag{Eq. A-15}$$

Back substitution of Eq. A-14 and Eq. A-15 into Eq. A-10 and Eq. A-12 results in the formulas for the in-plane strains and stresses:

$$\begin{aligned}
 \varepsilon_x &= \frac{N_x}{E \cdot h} + 12 \cdot \frac{M_x}{E \cdot h^3} \cdot z & \sigma_x &= \frac{N_x}{h} + 12 \cdot \frac{M_x}{h^3} \cdot z \\
 \varepsilon_y &= -\nu \cdot \varepsilon_x & \sigma_y &= 0 \\
 \gamma_{xy} &= 0 & \tau_{xy} &= 0
 \end{aligned}
 \tag{Eq. A-16}$$

Eq. A-16 clearly shows that for isotropic materials the stress components  $\sigma_y$  and  $\tau_{xy}$  are zero through the entire thickness, while  $\sigma_x$  varies linearly with the z-coordinate. Notice that strains (and curvature) in y-direction are not zero due to the Poisson's effect.

Now, consider a beam under transverse loading. Eq. A-6 gives the relationship between the normal stresses in x-direction and the shear stresses through the thickness. Substitution of Eq. A-16 into Eq. A-6 gives:

$$\frac{\partial \tau_{xz}}{\partial z} = -\frac{\partial N_x}{\partial x} \cdot \frac{1}{h} - 12 \cdot \frac{\partial M_x}{\partial x} \cdot \frac{1}{h^3} \cdot z$$

With the assumption that no forces are applied along the surface (lateral loading only), Eq. A-3 remains valid and we find:

$$\frac{\partial \tau_{xz}}{\partial z} = -12 \cdot Q_x \cdot \frac{1}{h^3} \cdot z$$

With the boundary condition that the shear stress at the outer surface is zero (no forces applied along the surface), we find:

$$\tau_{xz} = \frac{3 Q_x}{2 h} \cdot \left( 1 - \left( \frac{2 \cdot z}{h} \right)^2 \right)$$

With Eq. A-3 the two other through thickness stress components can be found as well:

$$\begin{aligned} \frac{\partial \tau_{yz}}{\partial z} &= 0 \\ \frac{\partial \sigma_z}{\partial z} &= \frac{3}{2} \cdot \frac{\partial Q_x}{\partial x} \cdot \left( 4 \cdot \frac{1}{h^3} \cdot z^2 - \frac{1}{h} \right) \end{aligned}$$

And applying the proper boundary conditions results in:

$$\begin{aligned} \tau_{yz} &= 0 \\ \sigma_z &= \frac{1}{2} \cdot p \cdot \left( 1 + 3 \cdot \frac{z}{h} - 4 \cdot \left( \frac{z}{h} \right)^3 \right) \end{aligned}$$

Concluding, the following equations are found for the through-thickness stresses:

$$\begin{aligned} \sigma_z &= \frac{1}{2} \cdot p \cdot \left( 1 + 3 \cdot \frac{z}{h} - 4 \cdot \left( \frac{z}{h} \right)^3 \right) \\ \tau_{xz} &= \frac{3 Q_x}{2 h} \cdot \left( 1 - \left( \frac{2 \cdot z}{h} \right)^2 \right) \\ \tau_{yz} &= 0 \end{aligned}$$

Eq. A-17



### A.3 Implementation of CPT for composite materials

In principle, for the beam consisting of composite materials the same procedure can be followed as for the isotropic one. However, the equations become more complex as a layer-wise approach has to be followed. In the composite case Eq. A-8 transforms in:

$$\begin{aligned}
 N_x &= \sum_{k=1}^n \int_{z_{k-1}}^{z_k} \sigma_x^{(k)} \cdot dz \\
 N_y &= \sum_{k=1}^n \int_{z_{k-1}}^{z_k} \sigma_y^{(k)} \cdot dz \\
 N_{xy} &= \sum_{k=1}^n \int_{z_{k-1}}^{z_k} \tau_{xy}^{(k)} \cdot dz
 \end{aligned}
 \tag{Eq. A-18}$$

Eq. A-9 becomes:

$$\begin{aligned}
 M_x &= \sum_{k=1}^n \int_{z_{k-1}}^{z_k} \sigma_x^{(k)} \cdot z \cdot dz \\
 M_y &= \sum_{k=1}^n \int_{z_{k-1}}^{z_k} \sigma_y^{(k)} \cdot z \cdot dz \\
 M_{xy} &= \sum_{k=1}^n \int_{z_{k-1}}^{z_k} \tau_{xy}^{(k)} \cdot z \cdot dz
 \end{aligned}
 \tag{Eq. A-19}$$

The parameter  $k$  is the ply number, starting at 1 and ending at ply  $n$ . The coordinate  $z = 0$  is located in the middle of the laminate,  $z_0$  is located at the bottom and  $z_n$  at the top.

Eq. A-10 remains the same; the total strain still consists of a component due to mid-plane deformation and a component due to bending/curvature. However, Eq. A-12 has to be modified, because the layer stress depends on the individual layer stiffness and orientation:

$$\begin{Bmatrix} \sigma_x \\ \sigma_y \\ \tau_{xy} \end{Bmatrix}_{(k)} = [\bar{C}]_{(k)} \cdot \begin{Bmatrix} \varepsilon_x \\ \varepsilon_y \\ \gamma_{xy} \end{Bmatrix}
 \tag{Eq. A-20}$$

In which:

$$[\bar{C}]_{(k)} = [T]_{(k)}^{-1} \cdot [C]_{(k)} \cdot [T]_{(k)}^{-T}$$

$$[C]_{(k)} = \begin{bmatrix} \frac{E_1}{1-\nu_{12} \cdot \nu_{21}} & \frac{\nu_{12} \cdot E_2}{1-\nu_{12} \cdot \nu_{21}} & 0 \\ & \frac{E_2}{1-\nu_{12} \cdot \nu_{21}} & 0 \\ & & G_{12} \end{bmatrix}$$

$$[T]_{(k)} = \begin{bmatrix} m^2 & n^2 & 2mn \\ n^2 & m^2 & -2mn \\ -mn & mn & m^2 - n^2 \end{bmatrix}$$

with  $m = \cos \varphi$  and  $n = \sin \varphi$ .

$[C]_{(k)}$  is the stiffness matrix of the  $k^{\text{th}}$  ply in its local ply coordinate frame (along the fibres).

$[T]_{(k)}$  is a transformation matrix, with  $\varphi$  being the ply angle with respect to the global material coordinate frame.

Substitution of Eq. A-10 in Eq. A-20 and next into Eq. A-18 and Eq. A-19 results in:

$$\begin{cases} N_x \\ N_y \\ N_{xy} \end{cases} = \sum_{k=1}^n [\bar{C}]_{(k)} \cdot (z_k - z_{k-1}) \cdot \begin{cases} \bar{\varepsilon}_x \\ \bar{\varepsilon}_y \\ \bar{\gamma}_{xy} \end{cases} + \frac{1}{2} \cdot \sum_{k=1}^n [\bar{C}]_{(k)} \cdot (z_k^2 - z_{k-1}^2) \cdot \begin{cases} \bar{\kappa}_x \\ \bar{\kappa}_y \\ 2 \cdot \bar{\kappa}_{xy} \end{cases}$$

$$\begin{cases} M_x \\ M_y \\ M_{xy} \end{cases} = \frac{1}{2} \cdot \sum_{k=1}^n [\bar{C}]_{(k)} \cdot (z_k^2 - z_{k-1}^2) \cdot \begin{cases} \bar{\varepsilon}_x \\ \bar{\varepsilon}_y \\ \bar{\gamma}_{xy} \end{cases} + \frac{1}{3} \cdot \sum_{k=1}^n [\bar{C}]_{(k)} \cdot (z_k^3 - z_{k-1}^3) \cdot \begin{cases} \bar{\kappa}_x \\ \bar{\kappa}_y \\ 2 \cdot \bar{\kappa}_{xy} \end{cases}$$

This can be rewritten to the well-known formula according to Classical Laminate Theory:

$$\begin{cases} N_x \\ N_y \\ N_{xy} \\ M_x \\ M_y \\ M_{xy} \end{cases} = \begin{bmatrix} A_{11} & A_{12} & A_{16} & B_{11} & B_{12} & B_{16} \\ A_{21} & A_{22} & A_{26} & B_{21} & B_{22} & B_{26} \\ A_{61} & A_{62} & A_{66} & B_{61} & B_{62} & B_{66} \\ \hline B_{11} & B_{12} & B_{16} & D_{11} & D_{12} & D_{16} \\ B_{21} & B_{22} & B_{26} & D_{21} & D_{22} & D_{26} \\ B_{61} & B_{62} & B_{66} & D_{61} & D_{62} & D_{66} \end{bmatrix} \cdot \begin{cases} \bar{\varepsilon}_x \\ \bar{\varepsilon}_y \\ \bar{\gamma}_{xy} \\ \bar{\kappa}_x \\ \bar{\kappa}_y \\ 2 \cdot \bar{\kappa}_{xy} \end{cases}$$

Eq. A-21

With:

$$\begin{aligned}
 [A] &= \sum_{k=1}^n [\bar{C}]_{(k)} \cdot (z_k - z_{k-1}) \\
 [B] &= \frac{1}{2} \cdot \sum_{k=1}^n [\bar{C}]_{(k)} \cdot (z_k^2 - z_{k-1}^2) \\
 [D] &= \frac{1}{3} \cdot \sum_{k=1}^n [\bar{C}]_{(k)} \cdot (z_k^3 - z_{k-1}^3)
 \end{aligned}$$

Inversion of the  $ABD$ -matrix, here denoted as  $abd$  with components  $a_{ij}$ ,  $b_{ij}$ , and  $d_{ij}$ , gives the strains and curvatures as a function of the in-plane loads and bending loads:

$$\begin{Bmatrix} \bar{\varepsilon}_x \\ \bar{\varepsilon}_y \\ \bar{\gamma}_{xy} \\ \bar{\kappa}_x \\ \bar{\kappa}_y \\ 2 \cdot \bar{\kappa}_{xy} \end{Bmatrix} = \begin{bmatrix} a_{11} & a_{12} & a_{16} & \vdots & b_{11} & b_{12} & b_{16} \\ a_{21} & a_{22} & a_{26} & \vdots & b_{21} & b_{22} & b_{26} \\ a_{61} & a_{62} & a_{66} & \vdots & b_{61} & b_{62} & b_{66} \\ b_{11} & b_{12} & b_{16} & \vdots & d_{11} & d_{12} & d_{16} \\ b_{21} & b_{22} & b_{26} & \vdots & d_{21} & d_{22} & d_{26} \\ b_{61} & b_{62} & b_{66} & \vdots & d_{61} & d_{66} & d_{66} \end{bmatrix} \cdot \begin{Bmatrix} N_x \\ N_y \\ N_{xy} \\ M_x \\ M_y \\ M_{xy} \end{Bmatrix}$$

As all applied loads in y-direction are assumed zero, this reduces to:

$$\begin{Bmatrix} \bar{\varepsilon}_x \\ \bar{\varepsilon}_y \\ \bar{\gamma}_{xy} \\ \bar{\kappa}_x \\ \bar{\kappa}_y \\ 2 \cdot \bar{\kappa}_{xy} \end{Bmatrix} = \begin{Bmatrix} a_{11} \\ a_{21} \\ a_{61} \\ b_{11} \\ b_{21} \\ b_{61} \end{Bmatrix} \cdot N_x + \begin{Bmatrix} b_{11} \\ b_{21} \\ b_{61} \\ d_{11} \\ d_{21} \\ d_{61} \end{Bmatrix} \cdot M_x$$

Now, the in-plane strains and stresses can be calculated in both the global coordinate system and in the local ply coordinate system (at any location through the thickness):

$$\begin{Bmatrix} \varepsilon_x \\ \varepsilon_y \\ \gamma_{xy} \end{Bmatrix} = \begin{Bmatrix} a_{11} + b_{11} \cdot z \\ a_{21} + b_{21} \cdot z \\ a_{61} + b_{61} \cdot z \end{Bmatrix} \cdot N_x + \begin{Bmatrix} b_{11} + d_{11} \cdot z \\ b_{21} + d_{21} \cdot z \\ b_{61} + d_{61} \cdot z \end{Bmatrix} \cdot M_x$$

$$\begin{Bmatrix} \varepsilon_1 \\ \varepsilon_2 \\ \gamma_{12} \end{Bmatrix}_{(k)} = [T]_{(k)}^{-T} \cdot \begin{Bmatrix} \varepsilon_x \\ \varepsilon_y \\ \gamma_{xy} \end{Bmatrix}$$

$$\begin{Bmatrix} \sigma_x \\ \sigma_y \\ \tau_{xy} \end{Bmatrix}_{(k)} = [\bar{C}]_{(k)} \cdot \begin{Bmatrix} \varepsilon_x \\ \varepsilon_y \\ \gamma_{xy} \end{Bmatrix}$$

$$\begin{Bmatrix} \sigma_1 \\ \sigma_2 \\ \tau_{12} \end{Bmatrix}_{(k)} = [C]_{(k)} \cdot \begin{Bmatrix} \varepsilon_1 \\ \varepsilon_2 \\ \gamma_{12} \end{Bmatrix}_{(k)}$$

Eq. A-22

The through-thickness stresses can be calculated by combining Eq. A-22, Eq. A-6 and Eq. A-3:

$$\left( \frac{\partial \tau_{xz}}{\partial z} \right)_{(k)} = - \left( \bar{C}_{11(k)} \cdot (b_{11} + d_{11} \cdot z) + \bar{C}_{12(k)} \cdot (b_{21} + d_{21} \cdot z) + \bar{C}_{16(k)} \cdot (b_{61} + d_{61} \cdot z) \right) \cdot Q_x$$

$$\left( \frac{\partial \tau_{yz}}{\partial z} \right)_{(k)} = - \left( \bar{C}_{61(k)} \cdot (b_{11} + d_{11} \cdot z) + \bar{C}_{62(k)} \cdot (b_{21} + d_{21} \cdot z) + \bar{C}_{66(k)} \cdot (b_{61} + d_{61} \cdot z) \right) \cdot Q_x$$

$$\left( \frac{\partial \sigma_z}{\partial z} \right)_{(k)} = - \left( \frac{\partial \tau_{xz}}{\partial x} \right)_{(k)}$$

With the boundary condition of zero shear stresses at the outer surface, one can deduce:

$$\tau_{xz}^{(k)} = \sum_{j=1}^{k-1} \int_{z_{j-1}}^{z_j} \left( \frac{\partial \tau_{xz}}{\partial z} \right)_{(j)} \cdot dz + \int_{z_{k-1}}^z \left( \frac{\partial \tau_{xz}}{\partial z} \right)_{(k)} \cdot dz$$

$$\tau_{yz}^{(k)} = \sum_{j=1}^{k-1} \int_{z_{j-1}}^{z_j} \left( \frac{\partial \tau_{yz}}{\partial z} \right)_{(j)} \cdot dz + \int_{z_{k-1}}^z \left( \frac{\partial \tau_{yz}}{\partial z} \right)_{(k)} \cdot dz$$

$$\sigma_z^{(k)} = - \sum_{j=1}^{k-1} \int_{z_{j-1}}^{z_j} \left( \frac{\partial \tau_{xz}}{\partial x} \right)_{(j)} \cdot dz - \int_{z_{k-1}}^z \left( \frac{\partial \tau_{xz}}{\partial x} \right)_{(k)} \cdot dz$$

Note: for the first ply ( $k = 1$ ) the sum  $\sum_{j=1}^{k-1}$  does not exist and should not be executed.

Integration of these equations results in:

$$\begin{aligned}\tau_{xz}^{(k)} = & - \sum_{j=1}^{k-1} \left\{ \left( \bar{C}_{11(j)} \cdot b_{11} + \bar{C}_{12(j)} \cdot b_{21} + \bar{C}_{16(j)} \cdot b_{61} \right) \cdot (z_j - z_{j-1}) \right. \\ & + \frac{1}{2} \cdot \left( \bar{C}_{11(j)} \cdot d_{11} + \bar{C}_{12(j)} \cdot d_{21} + \bar{C}_{16(j)} \cdot d_{61} \right) \cdot (z_j^2 - z_{j-1}^2) \left. \right\} \cdot Q_x \\ & - \left\{ \left( \bar{C}_{11(k)} \cdot b_{11} + \bar{C}_{12(k)} \cdot b_{21} + \bar{C}_{16(k)} \cdot b_{61} \right) \cdot (z - z_{k-1}) \right. \\ & + \frac{1}{2} \cdot \left( \bar{C}_{11(k)} \cdot d_{11} + \bar{C}_{12(k)} \cdot d_{21} + \bar{C}_{16(k)} \cdot d_{61} \right) \cdot (z^2 - z_{k-1}^2) \left. \right\} \cdot Q_x\end{aligned}$$

$$\begin{aligned}\tau_{yz}^{(k)} = & - \sum_{j=1}^{k-1} \left\{ \left( \bar{C}_{61(j)} \cdot b_{11} + \bar{C}_{62(j)} \cdot b_{21} + \bar{C}_{66(j)} \cdot b_{61} \right) \cdot (z_j - z_{j-1}) \right. \\ & + \frac{1}{2} \cdot \left( \bar{C}_{61(j)} \cdot d_{11} + \bar{C}_{62(j)} \cdot d_{21} + \bar{C}_{66(j)} \cdot d_{61} \right) \cdot (z_j^2 - z_{j-1}^2) \left. \right\} \cdot Q_x \\ & - \left\{ \left( \bar{C}_{61(k)} \cdot b_{11} + \bar{C}_{62(k)} \cdot b_{21} + \bar{C}_{66(k)} \cdot b_{61} \right) \cdot (z - z_{k-1}) \right. \\ & + \frac{1}{2} \cdot \left( \bar{C}_{61(k)} \cdot d_{11} + \bar{C}_{62(k)} \cdot d_{21} + \bar{C}_{66(k)} \cdot d_{61} \right) \cdot (z^2 - z_{k-1}^2) \left. \right\} \cdot Q_x\end{aligned}$$

Eq. A-23

$$\begin{aligned}\sigma_z^{(k)} = & \sigma_z^{(k-1)}(z = z_{k-1}) - \sum_{j=1}^{k-1} \left\{ \left( \bar{C}_{11(j)} \cdot b_{11} + \bar{C}_{12(j)} \cdot b_{21} + \bar{C}_{16(j)} \cdot b_{61} \right) \cdot (z_j - z_{j-1}) \right. \\ & + \frac{1}{2} \cdot \left( \bar{C}_{11(j)} \cdot d_{11} + \bar{C}_{12(j)} \cdot d_{21} + \bar{C}_{16(j)} \cdot d_{61} \right) \cdot (z_j^2 - z_{j-1}^2) \left. \right\} \cdot (z - z_{k-1}) \cdot p \\ & - \left\{ \frac{1}{2} \cdot \left( \bar{C}_{11(k)} \cdot b_{11} + \bar{C}_{12(k)} \cdot b_{21} + \bar{C}_{16(k)} \cdot b_{61} \right) \cdot (z - z_{k-1})^2 \right. \\ & + \frac{1}{6} \cdot \left( \bar{C}_{11(k)} \cdot d_{11} + \bar{C}_{12(k)} \cdot d_{21} + \bar{C}_{16(k)} \cdot d_{61} \right) \cdot (z - z_{k-1})^2 \cdot (z + 2 \cdot z_{k-1}) \left. \right\} \cdot p\end{aligned}$$

The last formula of Eq. A-23 shows that the normal stress  $\sigma_z$  in the  $k^{th}$  ply depends on the stress in the  $(k-1)^{th}$  ply at  $z = z_{k-1}$ , which in turn depends on the stress in the  $(k-2)^{th}$  ply at  $z = z_{k-2}$ , and so on. Numerically the implementation is quite easy even for a large number of plies. However, for an analytical determination of stresses it is better to rewrite this into:

For  $k = 1$  (First ply in the laminate):

$$\sigma_z^{(k)} = -\frac{1}{2} \cdot (\bar{C}_{11(k)} \cdot b_{11} + \bar{C}_{12(k)} \cdot b_{21} + \bar{C}_{16(k)} \cdot b_{61}) \cdot (z - z_{k-1})^2 + \frac{1}{6} \cdot (\bar{C}_{11(k)} \cdot d_{11} + \bar{C}_{12(k)} \cdot d_{21} + \bar{C}_{16(k)} \cdot d_{61}) \cdot (z - z_{k-1})^2 \cdot (z + 2 \cdot z_{k-1}) \cdot p$$

For  $k = 2$  (Second ply in the laminate):

$$\begin{aligned} \sigma_z^{(k)} = & -\sum_{j=1}^{k-1} \left\{ \frac{1}{2} \cdot (\bar{C}_{11(j)} \cdot b_{11} + \bar{C}_{12(j)} \cdot b_{21} + \bar{C}_{16(j)} \cdot b_{61}) \cdot (z_j - z_{j-1})^2 \right. \\ & \left. + \frac{1}{6} \cdot (\bar{C}_{11(j)} \cdot d_{11} + \bar{C}_{12(j)} \cdot d_{21} + \bar{C}_{16(j)} \cdot d_{61}) \cdot (z_j - z_{j-1})^2 \cdot (z_j + 2 \cdot z_{j-1}) \right\} \cdot p \\ & -\sum_{j=1}^{k-1} \left\{ (\bar{C}_{11(j)} \cdot b_{11} + \bar{C}_{12(j)} \cdot b_{21} + \bar{C}_{16(j)} \cdot b_{61}) \cdot (z_j - z_{j-1}) \right. \\ & \left. + \frac{1}{2} \cdot (\bar{C}_{11(j)} \cdot d_{11} + \bar{C}_{12(j)} \cdot d_{21} + \bar{C}_{16(j)} \cdot d_{61}) \cdot (z_j^2 - z_{j-1}^2) \right\} \cdot (z - z_{k-1}) \cdot p \\ & - \left\{ \frac{1}{2} \cdot (\bar{C}_{11(k)} \cdot b_{11} + \bar{C}_{12(k)} \cdot b_{21} + \bar{C}_{16(k)} \cdot b_{61}) \cdot (z - z_{k-1})^2 \right. \\ & \left. + \frac{1}{6} \cdot (\bar{C}_{11(k)} \cdot d_{11} + \bar{C}_{12(k)} \cdot d_{21} + \bar{C}_{16(k)} \cdot d_{61}) \cdot (z - z_{k-1})^2 \cdot (z + 2 \cdot z_{k-1}) \right\} \cdot p \end{aligned}$$

For  $k \geq 3$  ( $k^{th}$  ply in the laminate):

$$\begin{aligned} \sigma_z^{(k)} = & -\sum_{i=2}^{k-1} \left\{ \sum_{j=1}^{i-1} \left\{ (\bar{C}_{11(j)} \cdot b_{11} + \bar{C}_{12(j)} \cdot b_{21} + \bar{C}_{16(j)} \cdot b_{61}) \cdot (z_j - z_{j-1}) \right. \right. \\ & \left. \left. + \frac{1}{2} \cdot (\bar{C}_{11(j)} \cdot d_{11} + \bar{C}_{12(j)} \cdot d_{21} + \bar{C}_{16(j)} \cdot d_{61}) \cdot (z_j^2 - z_{j-1}^2) \right\} \cdot (z_i - z_{i-1}) \right\} \cdot p \\ & -\sum_{j=1}^{k-1} \left\{ \frac{1}{2} \cdot (\bar{C}_{11(k)} \cdot b_{11} + \bar{C}_{12(k)} \cdot b_{21} + \bar{C}_{16(k)} \cdot b_{61}) \cdot (z_j - z_{j-1})^2 \right. \\ & \left. + \frac{1}{6} \cdot (\bar{C}_{11(k)} \cdot d_{11} + \bar{C}_{12(k)} \cdot d_{21} + \bar{C}_{16(k)} \cdot d_{61}) \cdot (z_j - z_{j-1})^2 \cdot (z_j + 2 \cdot z_{j-1}) \right\} \cdot p \\ & -\sum_{j=1}^{k-1} \left\{ (\bar{C}_{11(j)} \cdot b_{11} + \bar{C}_{12(j)} \cdot b_{21} + \bar{C}_{16(j)} \cdot b_{61}) \cdot (z_j - z_{j-1}) \right. \\ & \left. + \frac{1}{2} \cdot (\bar{C}_{11(j)} \cdot d_{11} + \bar{C}_{12(j)} \cdot d_{21} + \bar{C}_{16(j)} \cdot d_{61}) \cdot (z_j^2 - z_{j-1}^2) \right\} \cdot (z - z_{k-1}) \cdot p \\ & - \left\{ \frac{1}{2} \cdot (\bar{C}_{11(k)} \cdot b_{11} + \bar{C}_{12(k)} \cdot b_{21} + \bar{C}_{16(k)} \cdot b_{61}) \cdot (z - z_{k-1})^2 \right. \\ & \left. + \frac{1}{6} \cdot (\bar{C}_{11(k)} \cdot d_{11} + \bar{C}_{12(k)} \cdot d_{21} + \bar{C}_{16(k)} \cdot d_{61}) \cdot (z - z_{k-1})^2 \cdot (z + 2 \cdot z_{k-1}) \right\} \cdot p \end{aligned}$$

## Appendix B

Consider the three-point bending test on an isotropic beam and on a laminate, see figure B-1. As we are only interested in the distribution of stresses, in the determination of stresses the following transverse load is assumed:

$$\frac{Q_x}{h} = 1 \text{ N/mm}^2 \quad \text{or} \quad \frac{P}{2bh} = 1 \text{ N/mm}^2$$

The standard test configuration to determine the ILS strength is a laminate consisting of  $0^\circ$  plies only. For the shear stresses this results in the same stress distribution as in an isotropic beam, i.e. a perfectly parabolic distribution. However, for other lay-ups deviant distributions will be found. Two alternative lay-ups are shown in figure B-1, one for a beam with “soft” inner plies (e.g.  $90^\circ$  plies moved inward and  $0^\circ$  plies moved outward) and one for a beam with “soft” outer plies. The result is a blunter curve with a lower peak stress for the lay-up with “soft” inner plies and a more slender curve with a higher peak stress for the lay-up with “soft” outer plies. So for ILS test coupons with a lay-up deviant from the standard lay-up with  $0^\circ$  plies only, the standard formula of reference 3 can no longer be applied to calculate the shear stress.

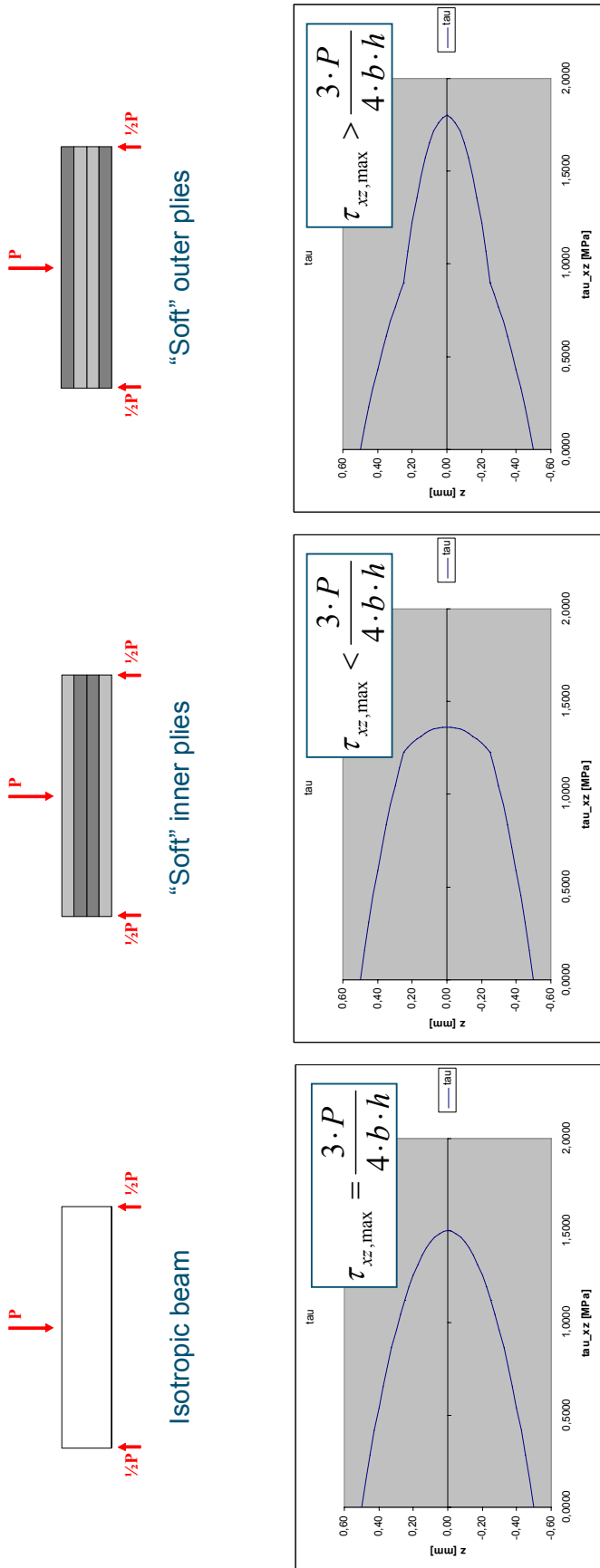


Fig. B-1 Transverse shear stresses due to three-point bending test on an isotropic beam and a layered beam



### Appendix C ILS failure stress in local ply directions

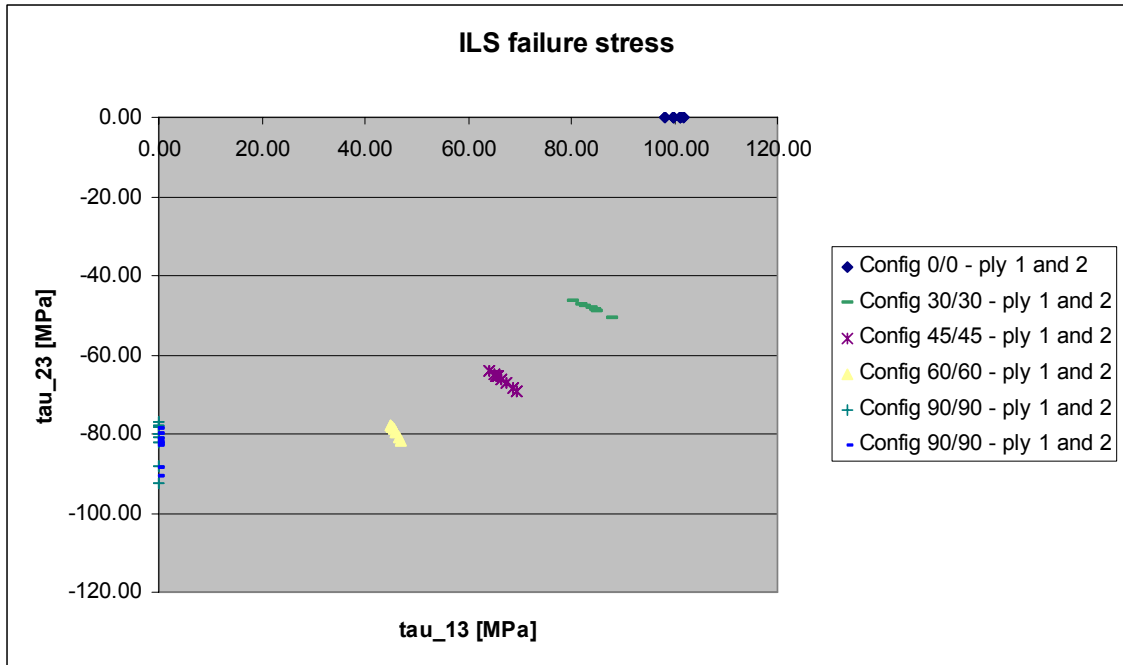


Fig. C-1 Failure stress in local ply directions for  $\theta/\theta$  interface

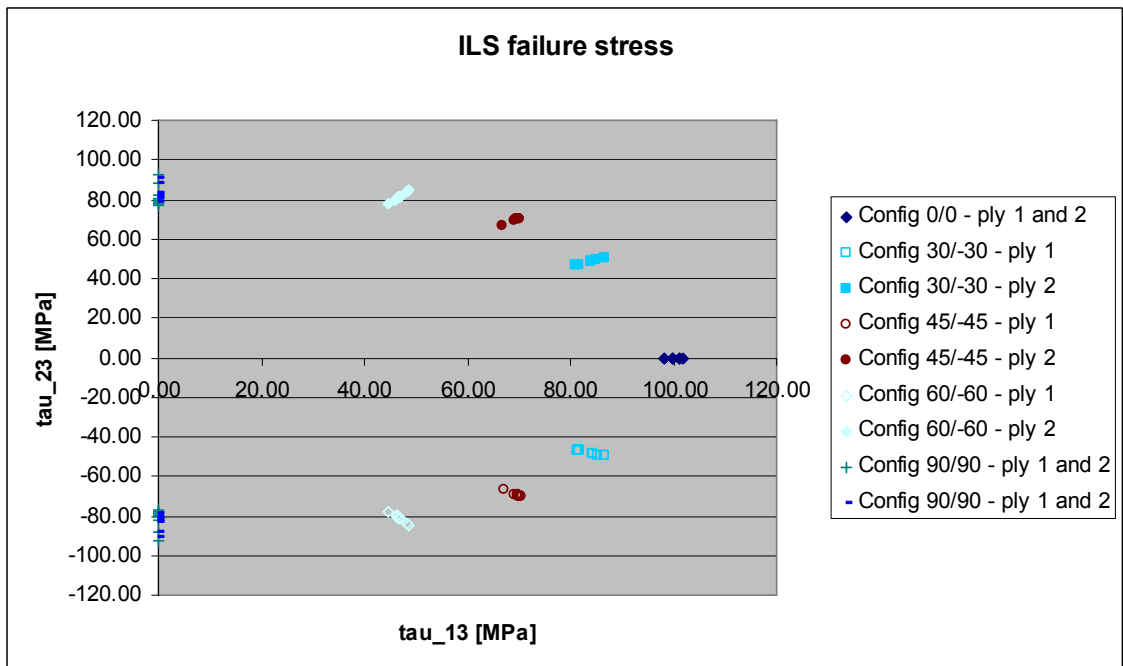


Fig. C-2 Failure stress in local ply directions for  $\theta/\theta$  interface

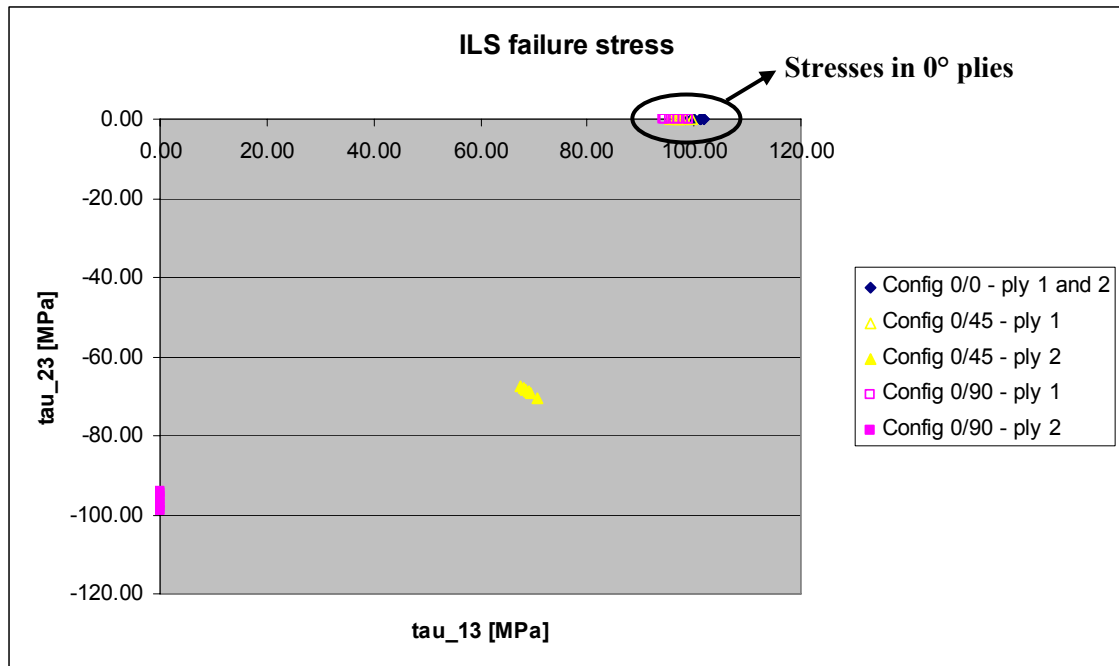


Fig. C-3 Failure stress in local ply directions for 0/θ interface

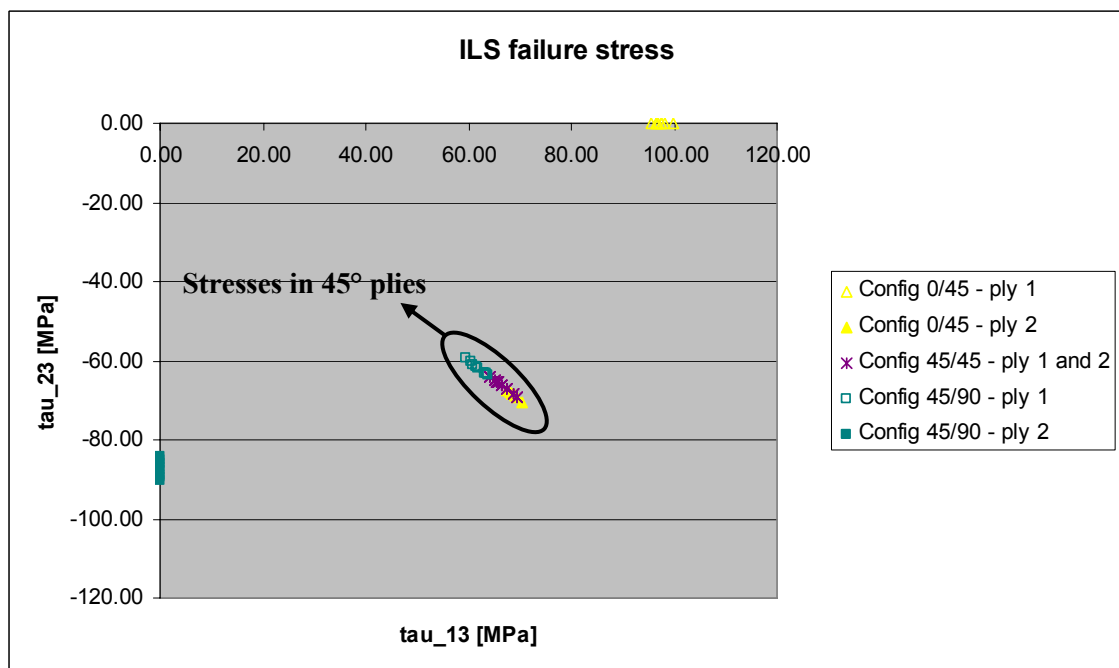


Fig. C-4 Failure stress in local ply directions for 45/θ interface

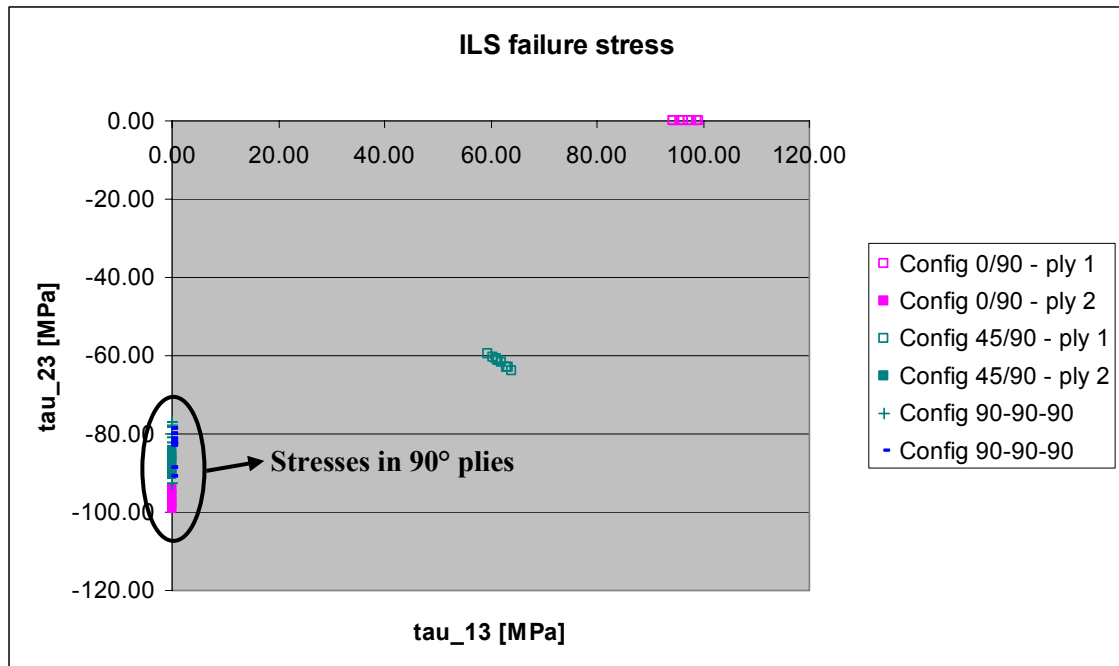


Fig. C-5 Failure stress in local ply directions for 90/ $\theta$  interface